2 SEISMOLOGY AND EARTHQUAKE GROUND MOTIONS

This report summarizes a preliminary study on the characteristics of the strong-motion recordings from the **M** 6.0 South Napa, California, Earthquake of August 24, 2014. The effort includes strong-motion data collection, data processing, metadata computation such as source-to-site distances, and estimates of site parameters such as V_{s30}. Strong motion recordings (PGA $\geq$0.30g) are reviewed at near-fault stations. Pseudo-Spectral Acceleration (PSA) values (5% damped) are compared to those estimated with the latest ground motion prediction equations (GMPEs) and current design spectra.

1.1 INTENSITY DISTRIBUTIONS

The South Napa Earthquake occurred on August 24, 2014 at 10:20:44 (UTC) in the West Napa fault zones. Figure 1 shows the ShakeMap from USGS website for this event (http://earthquake.usgs.gov/earthquakes/eventpage/nc72282711#shakemap, last accessed 09/10/2014). The hypocenter is located at the south end of Napa Valley of a depth of 10 km. Instrumental intensity measurements from ShakeMap were distributed along the Napa Valley with a maximum of IX at Napa Fire Station No. 3. The figure also shows the stations for which strong-motion data were processed for inclusion of the PEER strong motion database.

1.2 STRONG MOTION RECORDS

1.2.1 Acceleration Time Series Observations

Strong ground motions were downloaded from the Center for Engineering Strong Motion Data (CESMD) at the web site (http://strongmotioncenter.org/, last accessed 09/13/2014). A total of 214 three-component uncorrected digital accelerograms were downloaded. These records were processed following the PEER standard procedure (Ancheta et al. 2014), which includes inspection of record quality, selection of time windows, such as P-waves, S-waves, and coda waves, and component specific filter corner frequencies to optimize the usable frequency range.

Table 1 shows seven stations that recorded a median horizontal peak ground acceleration (PGA) (RotD50; Boore. 2010) greater than 0.3 g. Three stations in Table 1 are in the City of Napa, for which the arithmetic average of PGA was 0.40 g. The average PGA decreased to 0.07 g in the cities of Petaluma and Pinole, and less than 0.03 g in Berkeley and San Francisco.

Figure 2 shows the acceleration time series recorded at the stations listed in Table 1. Figure 2a, 2b, and 2c show the time series for Up-Down (UD), North-South (NS), and East-West (EW) components, respectively. The records from the Carquinez Bridge Geotechnical Array #1 shows high-frequency spikes and recorded the largest PGA of nearly 1.0 g in NS direction (Figure 2b). Napa, Fire station No. 3 shows a long-period pulse in EW direction (Figure 2c), and recorded the largest instrumental intensity of IX (Figure 1). Figure 2 also shows that all the records have a significant duration of less than 10 seconds

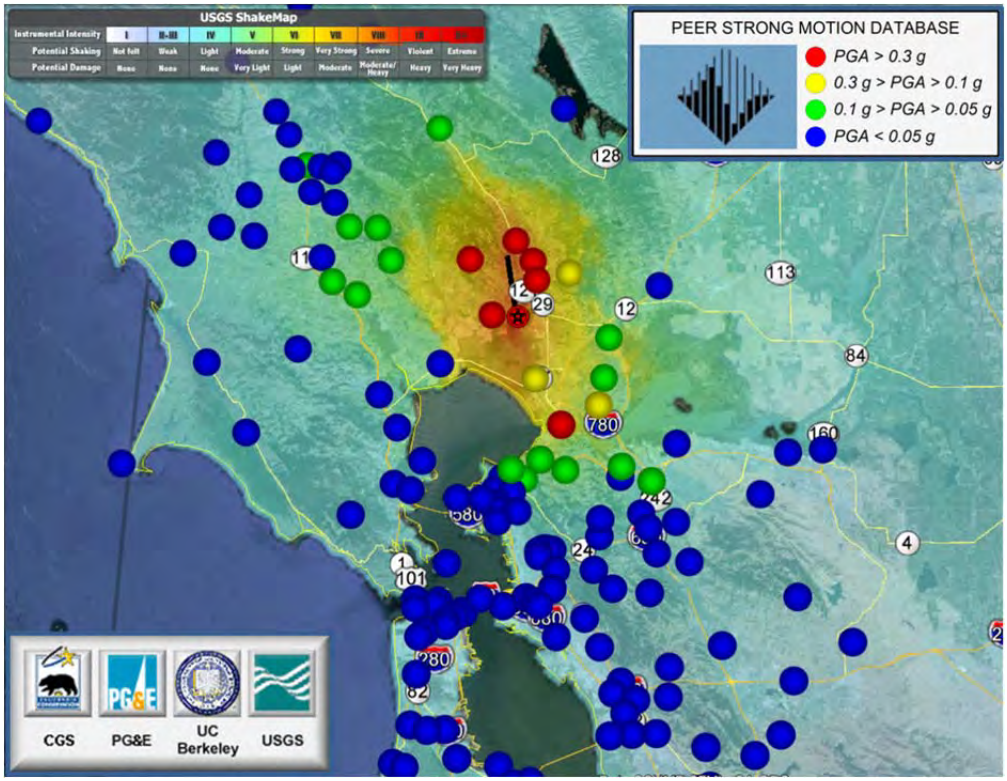

Figure 1 ShakeMap for South Napa Earthquake from the USGS overlaid with S strong motion stations processed by PEER

Table 1. Stations that recorded median PGA (RotD50) greater than 0.3 g

Station Name	Network [a]	Station ID	Latitude (deg)	Longitude (deg)	R_{rup} [b] (km)	V_{s30} [c] (m/s)	PGA (g)
Napa; Fire Station No. 3	USGS	1765	38.330	-122.318	2.6	332	0.42
Huichica Creek	NCSN	NHC	38.217	-122.358	3.9	217	0.31
Main St, Napa	NCSN	N016	38.299	-122.285	3.9	285	0.45
Napa – Napa College	CGS	68150	38.270	-122.277	4.1	339	0.34
Lovall Valley Loop Rd	NCSN	N019B	38.301	-122.402	6.1	710	0.35
Crockett – Carquinez Bridge Geotechnical Array #2	CGS	68259	38.055	-122.226	19.9	342	0.34
Crockett – Carquinez Bridge Geotechnical Array #1	CGS	68206	38.054	-122.225	20.0	342	0.70

a) CGS = California Geological Survey \ California Strong Motion Instrumentation Program, NCSN = USGS Northern California Seismic Network

b) Source-to-site distance based on Boatwright (2014) preliminary finite fault plane model

c) Estimated V_{s30}

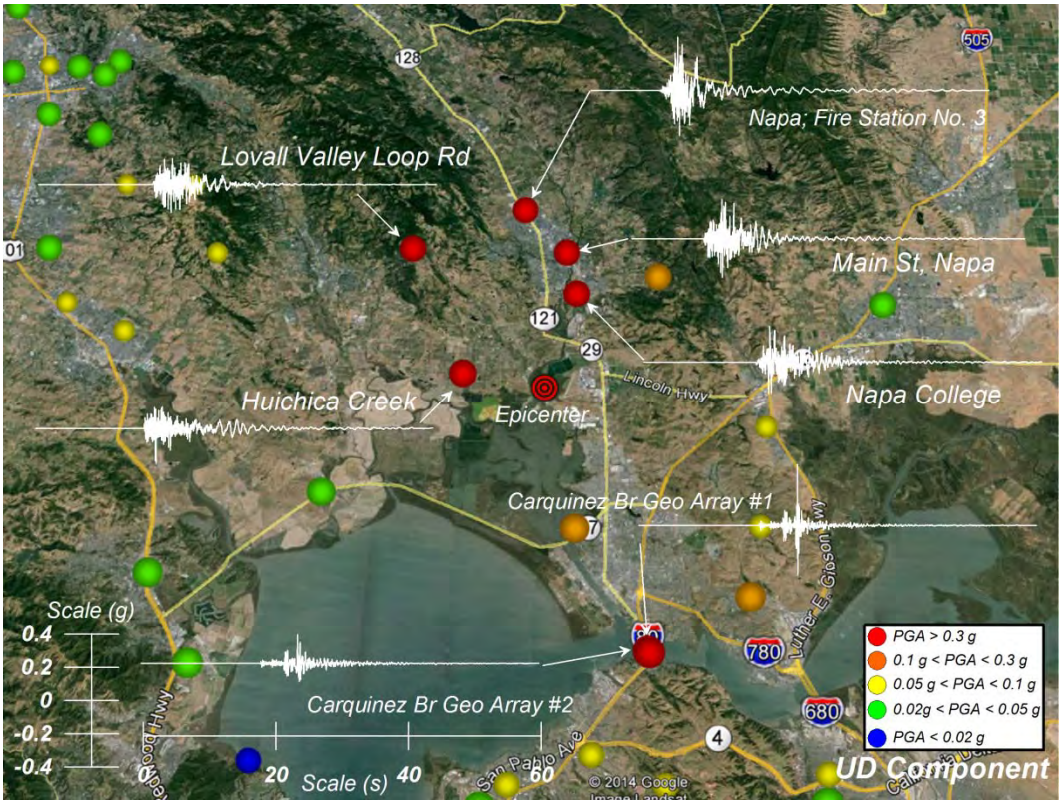

Figure 2a. Acceleration Time Series, UD Component

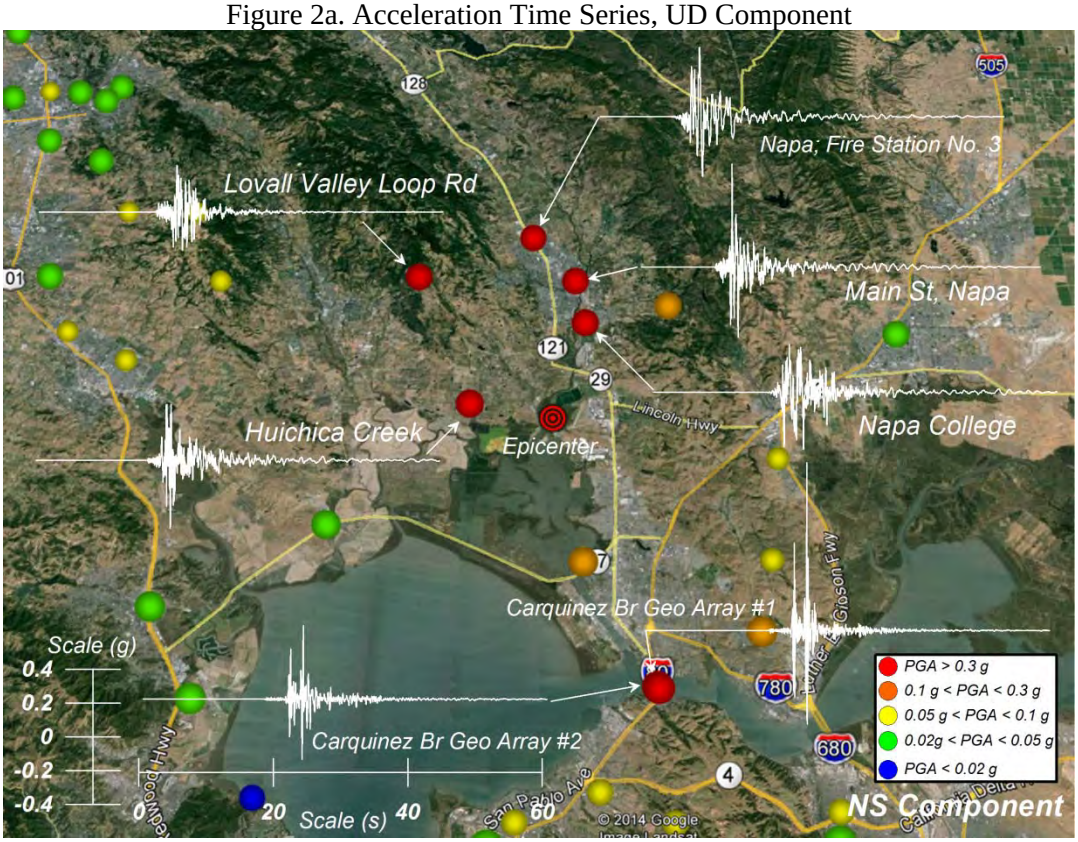

Figure 2b. Acceleration Time Series, NS Component

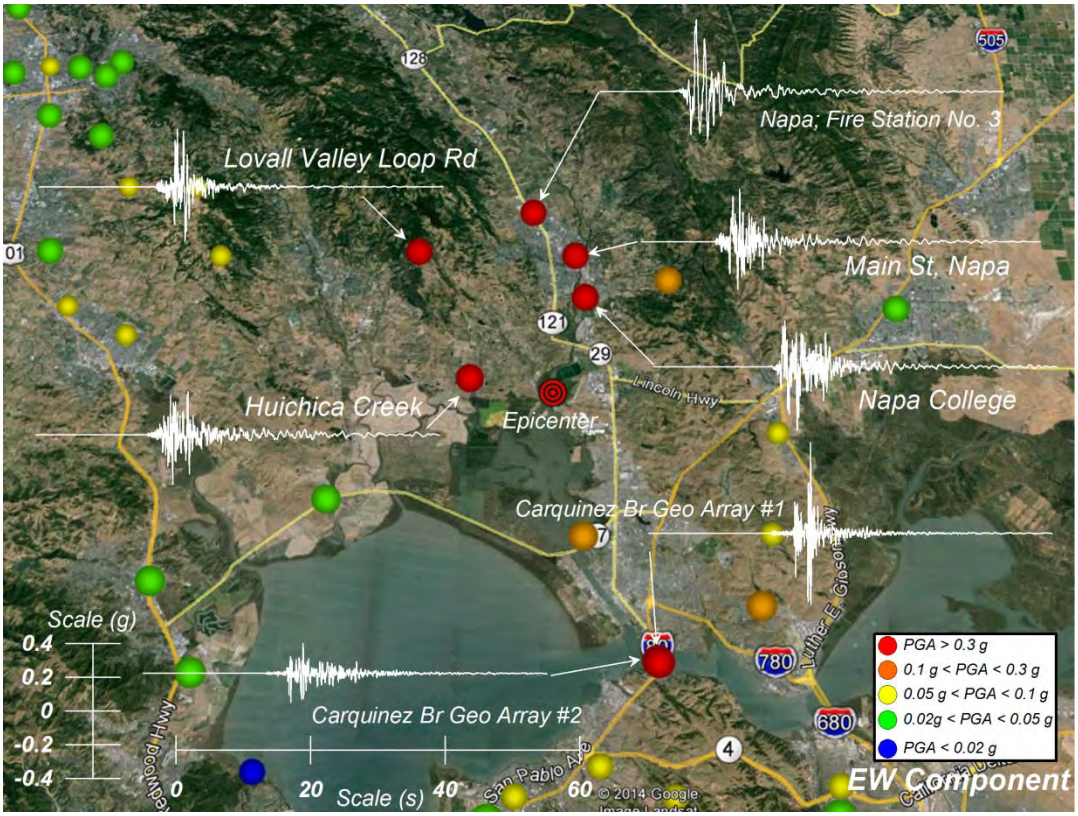

Figure 2c. Acceleration Time Series, EW Component

1.2.2 Near-Fault Pulse Observations

Pulse-like waveforms were observed in several of the velocity time series at the near-fault stations shown in Figure 2. On the basis of this observation, the horizontal components of near-fault velocity time series were rotated into fault-normal (FN) and fault-parallel (FP) orientations where the fault strike was taken as 155 degree (Figure 3). Maximum Peak Ground Velocity (PGV) was recorded as 84 cm/s in FP direction at Napa Fire Station No. 3. Based on visual inspection of Figure 3, Napa Fire Station No. 3 (FN, FP components), Lovall Valley Loop Rood (FN, FP components), Main St. (FN component), Huichica Creek (FP component), and Napa College (FN, FP components) show pulse-like waveforms in the velocity time series.

Appendix A Table 1 shows the recorded PGV (RotD50), expected PGVs and the periods by Bray et al. (2009) for these five stations. The Bray et al. (2009) relationship estimates a median PGV of about 50 to 60 cm/s for the fault-normal component of the five near-fault strong motion stations with a 16% to 84% range of about 35 to 85 cm/s. This captures the recorded near fault normal component PGVs fairly well. The period of the near-fault fault-normal velocity pulse was estimated to be within the range of 0.7 s to 2.0 s (16% to 84% values, respectively). The recorded velocity time series of the five near-fault records for the M6 South Napa earthquake contained shorter period velocity pulses within this estimated range, but they also contained longer period pulses significantly higher than this range. It is not clear if the longer period pulses were due to fault mechanism or site effects (e.g., deep basin response).

The following sections describe the characteristics of the velocity pulse near the fault evaluated by several different approaches.

1.2.2.1 Examination of Velocity Pulse by Hayden (2014) and Shahi (2013) Approaches

The presence of pulse-like motions in the near-fault region was studied through the examination of velocity records at five recording stations. Two methods were used to classify motions as pulse-like or non-pulse-like. The first scheme was proposed by Hayden et al. (2014), while the second classification scheme was proposed in Shahi (2013). Table 2 lists the recording stations examined and summarizes the results of the classification process. Plots of the resulting velocity records for the components with the highest "pulse-like tendencies" for each recording station for both the Hayden et al. (2014) and Shahi (2013) methods are provided in Appendix A.

For three of the five stations examined (Fire Station No. 3, Lovall Valley Loop Rd., and Huichica Creek) the two methods agree with regards to pulse classification. For the two remaining stations (Napa College and Main St. Napa) the two methods disagree with regards to the identification of a pulse-like motion. For the Napa College station, the Shahi (2013) scheme identifies a pulse, while the Hayden et al. (2014) method yields a pulse score of 25%, which is below the proposed pulse score threshold of 60%. The discrepancy between the two classifications for this station could be due to the presence of two significant cycles in the velocity time history, which downgrades the significant cycle sub-score that contributes to the overall pulse score in the Hayden et al. (2014) procedure. The discrepancy between the classification results for the Main St. Napa station is not as easily explained through the salient features of the velocity time series.

Importantly, the Huichica Creek station was in a backward directivity location and its maximum velocity and pulse component was roughly in the fault-parallel orientation. Three of the four remaining sites were in forward directivity locations and their maximum velocity and pulse components were within 30 degrees of the fault normal orientation.

Table 2: Results of Pulse Classification Methods

	Hayden et al. (2014)				Shahi (2013)		
Station Name	Pulse Score (%)	PPV[1] (cm/s)	Pulse Period (s)	Azimuth of Max PPV (°)	Pulse Identified	Azimuth of Max Pulse (°)	Pulse Period (s)
Fire Station No. 3	100	111	3.8	62	Yes	61.5	4.4
Huichica Creek	100	58.5	5.5	351	Yes	283.6	2.8
Lovall Valley Loop Rd.	100	64.3	3.9	61	Yes	20.7	3.6
Main St. Napa	92	62.3	3.4	56	No	29.7	3.9
Napa College	25	104	1.6	340	Yes	296.0	2.0

1) PPV = Peak-to-Peak Velocity (see Hayden et al. 2014)

1.2.2.2 Characterization of Near-fault Ground Motion Records by Lu and Panagiotou (2014)

This section presents a wavelet analysis of the ground motions recorded at two stations during the **M** 6 South Napa earthquake: Napa Fire Station No. 3 and Main St. recording stations. The originally recorded ground motion records were rotated (by Lu and Panagiotou) to the fault-normal (FN) and fault-parallel (FP) directions. The rotated ground acceleration and ground velocity histories, as well as the acceleration and displacement response spectra, for both components are shown in Appendix D Figure 1 and 2 for the Napa Fire Statiomn #3 and in Appendix D Figures 3 and 4 for the Main St. records. Both stations were expected to have been significantly affected by forward directivity.

The wavelet analysis was conducted using the cumulative pulse extraction (CPE) method described in Lu and Panagiotou (2014). The analysis was conducted in the velocity time domain and the order of the extracted pulses was determined based on the energy of the pulses ($CPE_{V,EN}$ method). For each motion, three pulses were extracted. The sum of the pulses in the time domain results in a representation of the ground motion. Appendix D Figures 1 to 4 show the extracted pulses in both the acceleration and the velocity time domain.

The Napa Fire Station No. 3 recordings include multiple strong pulses of significantly different predominant period T_P. The FP component (Appendix D Figure 1) exhibits the largest PGV which is the result of two pulses, one with $T_{P,1}$ = 1.1 s and another with $T_{P,2}$ = 3.9 s. The peaks of these two pulses are well correlated in the time domain. The FN component (Appendix D Figure 2) of the ground motion at Napa Fire Station No. 3 includes a strong pulse of $T_{P,1}$ = 1.9 s which determines the PGV of this motion. After that pulse a pulse with $T_{P,3}$ = 1.1 s follows in the time domain. The spectral demands for T larger than 3 s are dominated from the combination of the two pulses with $T_{P,1}$ =1.9 s and $T_{P,3}$ = 3.3 s. The FP component of the Main St. record (Appendix D Figure 3) exhibits a larger PGA than that of the FN component while the latter exhibits a larger PGV. The ground velocity waveform of the FN component is quite complex with the three pulses (T_{P1} = 3.1 s, $T_{P,2}$ = 1.2 s and $T_{P,3}$ = 0.6 s) to be highly correlated in the time domain.

1.2.1 Carquinez Bridge Records

This section discusses the time series recorded at the two Crockett – Carquinez Bridge Geotechnical Arrays by comparing the records along the source-to-site path and those from the three downhole arrays. The Geotechnical Arrays are a cooperative project of California Department of Transportation (Caltrans) and CSMIP.

The Crockett – Carquinez Bridge Geotechnical Array #1 recorded the largest PGA during the **M** 6 South Napa earthquake where the NS component reached approximately 1.0 g as shown in Figure 2a. Figure 4 shows the acceleration time series along strike direction from the epipocenter to the Carquinez Bridge. The recording at Carquinez Bridge Geotechnical Array #1 shows two high frequency spikes (approximately 10 Hz) after the S-wave arrival that have peak amplitudes of approximately 1.0 g in the North direction. Similar spikes were observed in the recordings at Carquinez Bridge Geotechnical Array #2, the Vallejo – Hwy 37/Napa River East Geotechnical Array, and at Napa College in Figure 4, although these amplitudes are smaller than those measured at the Carquinez Bridge Geotechnical Array #1. The record at Pinole Ridge did not show these spikes in the records. This observation may indicate that these spikes were amplified from the source to the Carquinez Bridge Geotechnical Array #1 site by path effects.

Figure 5 shows the downhole records for acceleration time series, 5%-damped Pseudo-Spectral Acceleration (PSA) and Fourier Amplitude Spectra (FAS) at Carquinez Bridge Geotechnical Array #1, #2, and Vallejo – Hwy. 37/Napa River East Geotechnical Array. Figures 5a and 5c show that the frequency content near 10 Hz were amplified through subsurface soil deposits of less than 20 m where Figure 5b shows that the frequency content near 3 Hz were amplified through subsurface soil deposit of less than 60 m. At all three arrays most of the amplification occurs between the middle sensor and the surface with less amplification between the deepest recording and the middle recording. The two high frequency spikes are observed after the direct S-wave arrival at all downhole arrays, these arrivals may be from S-waves radiated from other portions of the fault rupture to the north (e.g. http://earthquake.usgs.gov/earthquakes/eventpage/nc72282711#scientific_finite-fault).This observation may indicate that the large PGA observed at Carquinez Bridge could be a site effect caused by the soft soil deposits. These observations do not exclude the possibility of soil-structure interaction effects on the

measured recordings, because these time series were recorded near bridge abutments and structures. Additional study is needed to understand the effects of source, path, site, and nearby structures on these recordings.

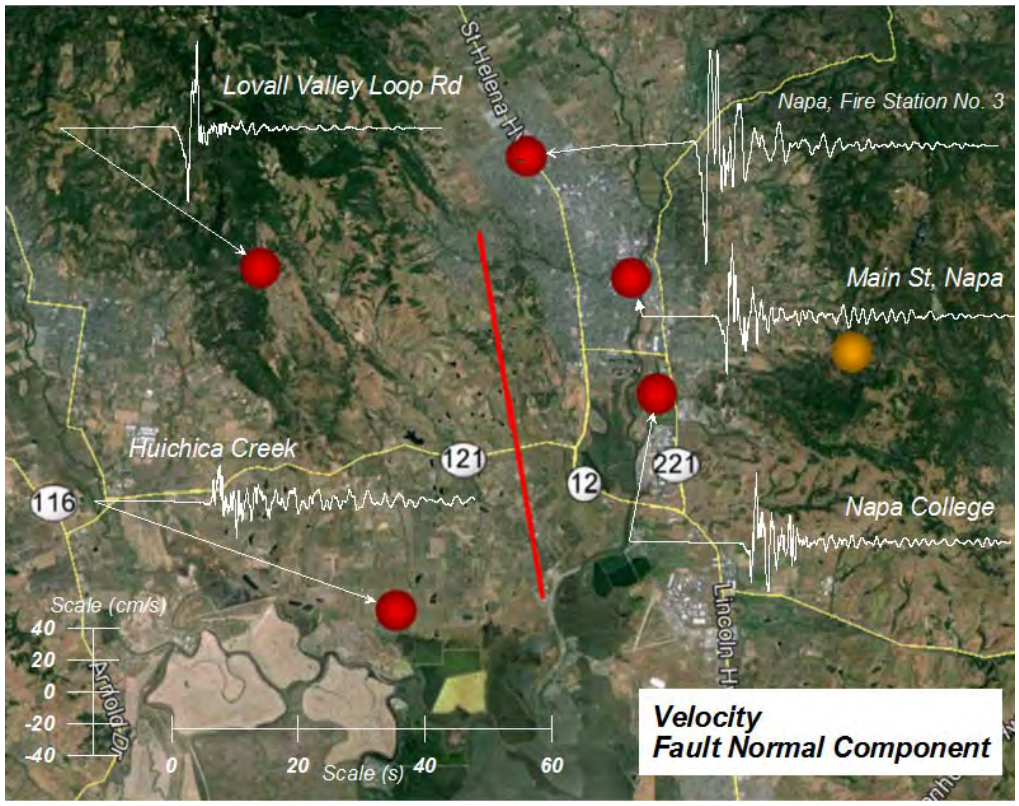

Figure 3a. Fault Normal Velocity Time Series

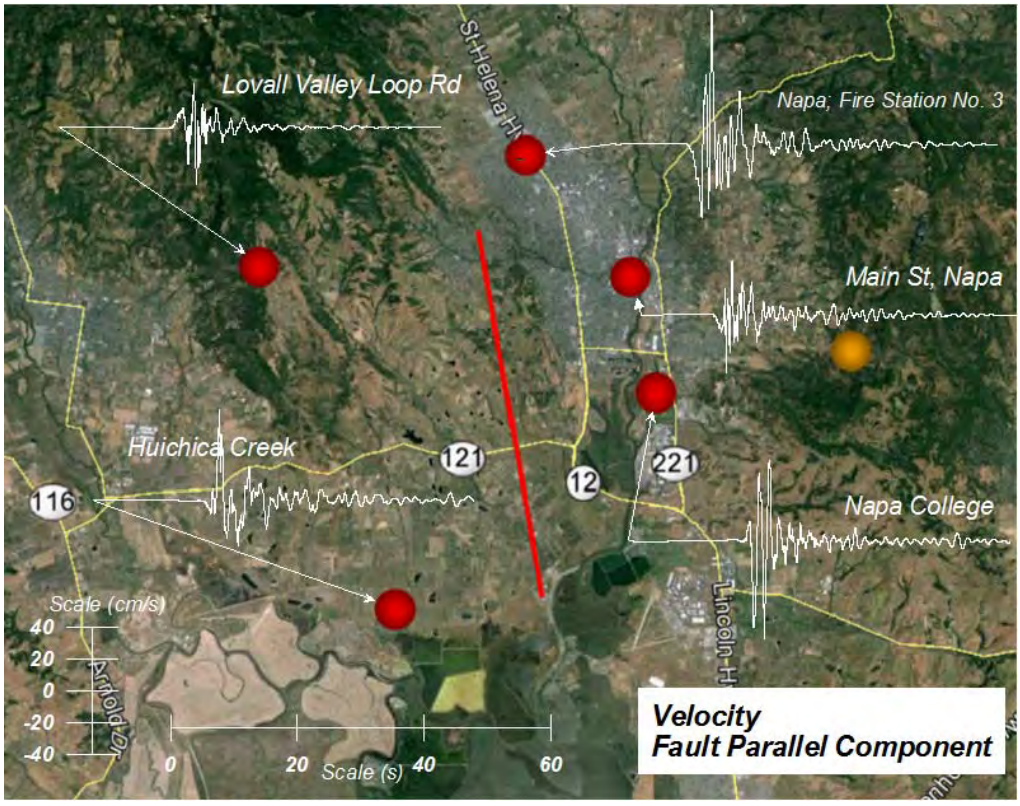

Figure 3b. Fault Parallel Velocity Time Series

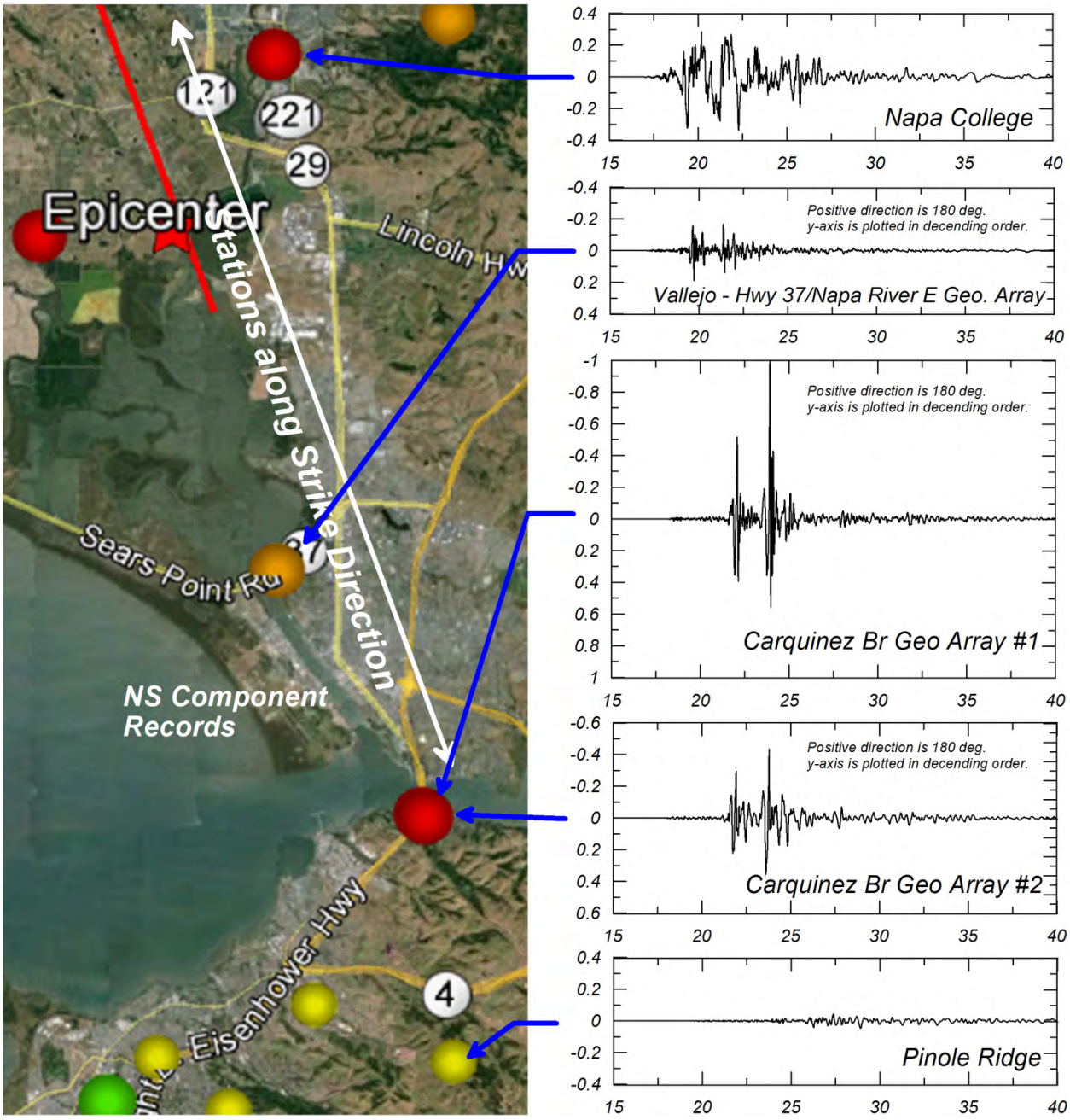

Figure 4. Acceleration time series along strike direction from source to Carquinez Bridge

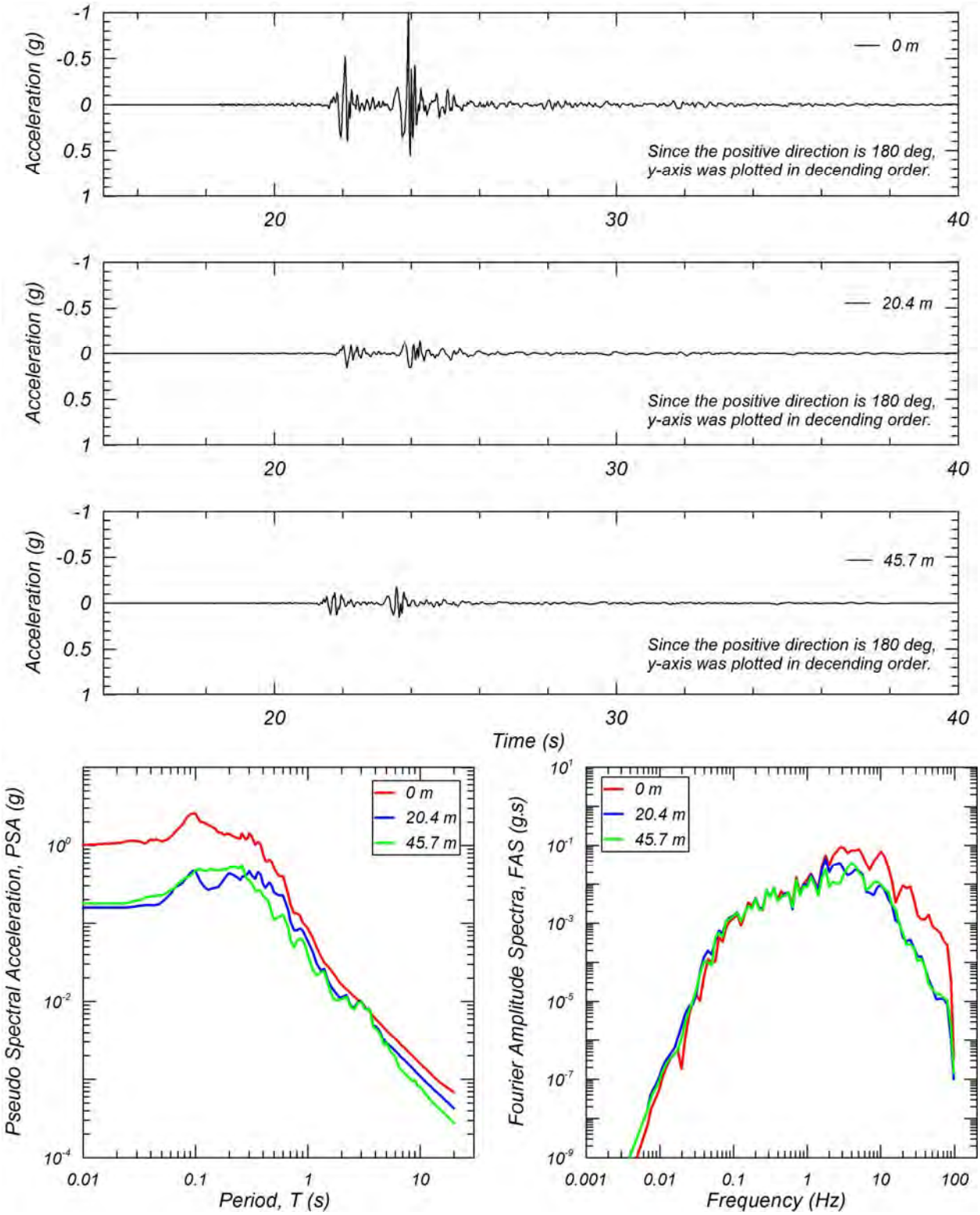

Figure 5a. Acceleration time series, 5% damped PSA, and FAS for Carquinez Bridge Geotechnical Array #1, NS Component

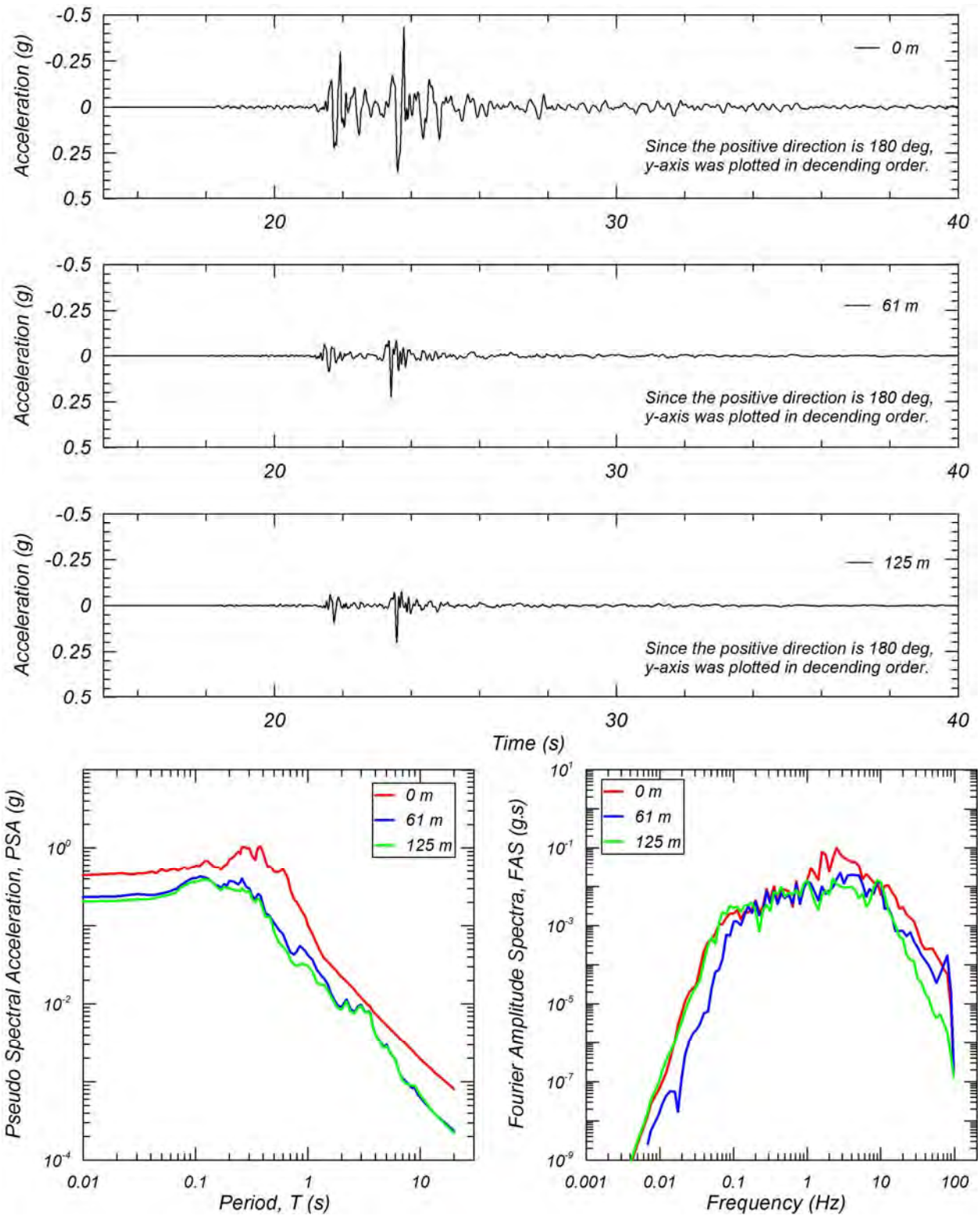

Figure 5b. Acceleration time series, 5% damped PSA, and FAS for Carquinez Bridge Geotechnical Array #2, NS Component

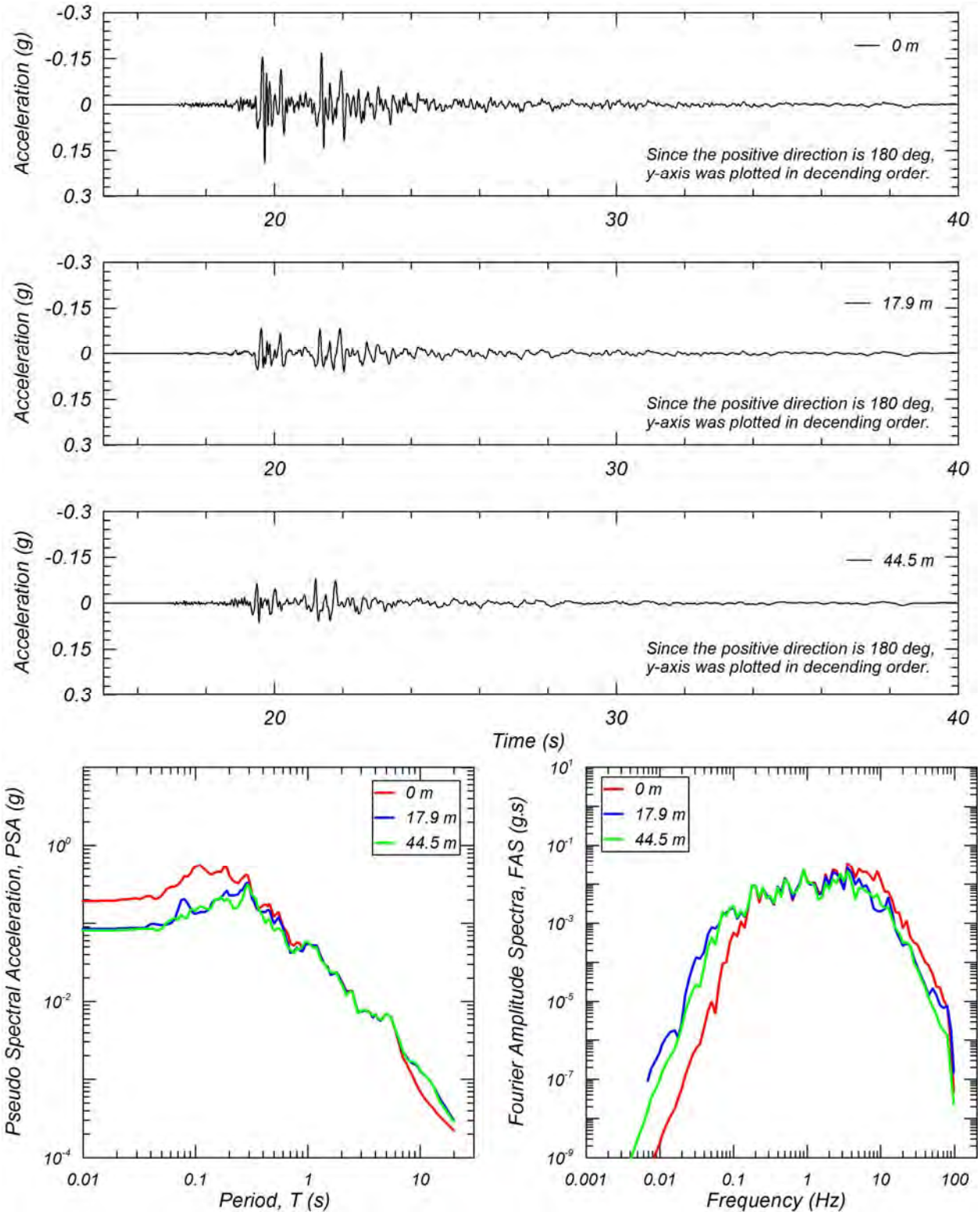

Figure 5c. Acceleration time series, 5% damped PSA, and FAS for Vallejo – Hwy 37/Napa River East Geotechnical Array, NS Component

1.3 ACCELERATION, VELOCITY AND DISPLACEMENT TIME SERIES

The acceleration, velocity, and displacement time series are plotted in Figure 6 for the NS component of Napa College Station. The figure also shows the Arias Intensity (AI), 5%-damped PSA, and FAS.

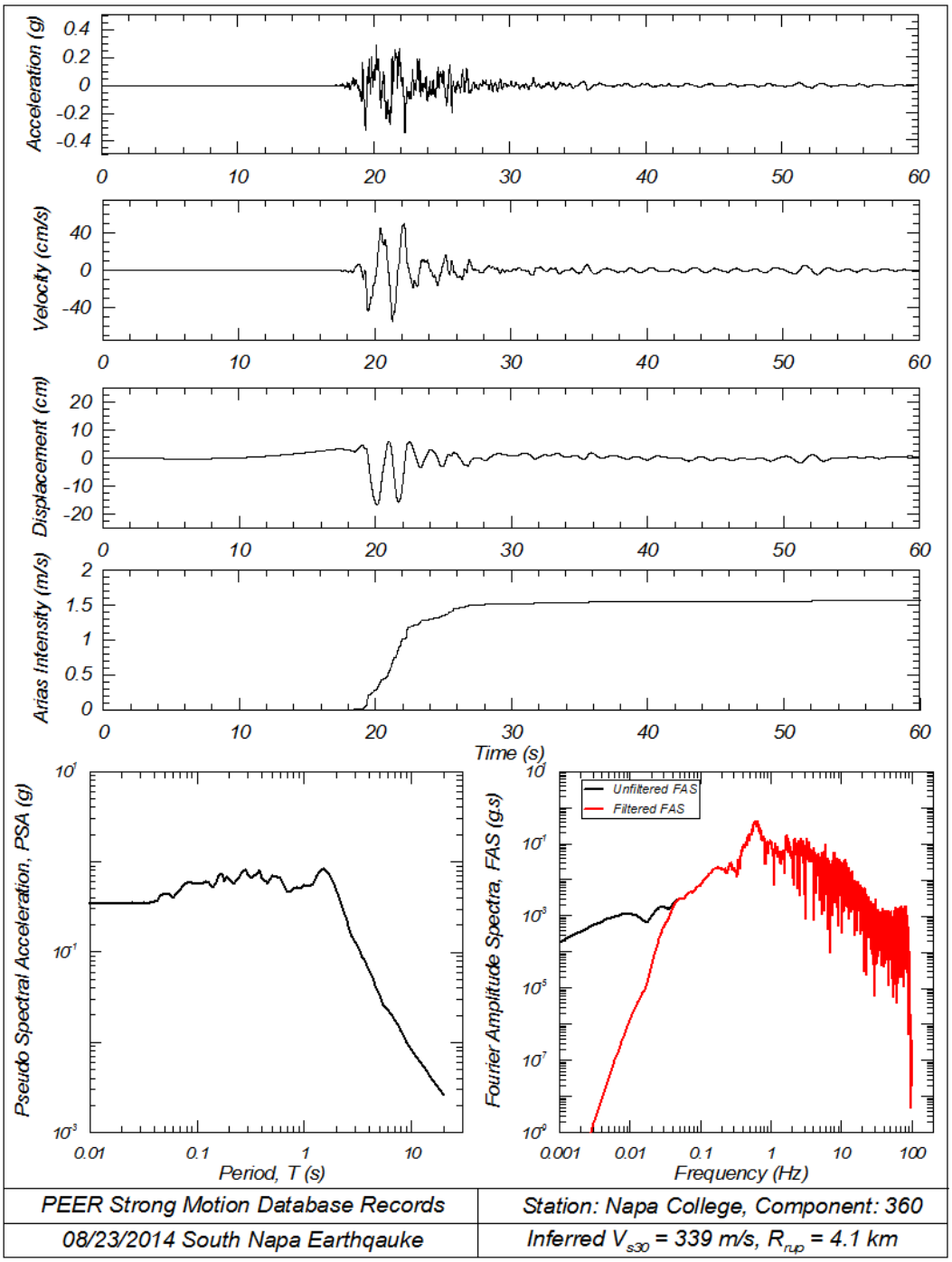

Figure 6. Summary of time series and spectra at Napa College Station (NS Component)

The PGA, PGV and AI recorded at this station were 0.339 g, 54.8 cm/s, and 1.56 m/s, respectively. The figure also shows the clear velocity pulse in the S-wave arrivals which was discussed in the previous section. The period of this waveform is approximately 1.5 s which is also seen in the pseudo-spectral acceleration (PSA) values (5% damped) in the figure. Similarly, the FAS has a peak amplitude near 0.7 Hz. Similar plots are presented in Appendix B for the other stations listed in Table 1.

1.4 COMPARISON TO GROUND-MOTION PREDICTION EQUATIONS

1.4.1 Fault Location and Recording Site Conditions

We reviewed the available surface slip and fault slip inversions and selected a preliminary preferred fault model for distance calculations. Fault mechanism and hypocenter location were obtained from the Northern California Earthquake Data Center (NCEDC) (http://www.ncedc.org/, last accessed 09/07/2014) (Table 3). The table shows that the earthquake fault mechanism is cstrike-slip based on the rake angle. Two preliminary finite fault models were available at the USGS website (http://earthquake.usgs.gov/earthquakes/eventpage/nc72282711#scientific_finite-fault, last accessed at 09/07/2014). One model inverts regional seismic waveforms for slip amplitude on the fault (Dreger, 2014). The second inverts regional GPS and InSAR data obtained by the USGS NEIC (Barnhart, 2014). Field observation of surface rupture are also available from the University of California, Davis (http://blogs.agu.org/tremblingearth/2014/08/30/earthquake-rupture-u-s-suburb/, last accessed at 09/07/2014) (Elliot 2014) The model using regional GPS and InSAR agree closely to the inversion model using regional seismic data regarding the depth and amount of peak slip. On the basis of these observations, we selected the finite fault model based on the inversion model using regional seismic data in Table 4 where rupture was extended to the ground surface based on the study (Boatwright 2014, http://earthquake.usgs.gov/product/shakemap/nc72282711/nc/1409779655706/download/boat_fault.txt, last accessed at 09/10/2014) that was based on observation of surface rupture. By using this preliminary fault model, the distance measures (R_{epi}, R_{hyp}, R_{rup}, R_{jb}, R_{sei}, and R_x) were computed for all 214 records. The strike and dip of the selected finite fault model in Table 4 are 170 and 90, respectively. These values are different from those by NCEDC in Table 3. However, we preferred the preliminary fault model in Table 4, because it will potentially provide distances with smaller errors taking into account the uncertainties in dip direction and the number of rectangular fault segments

Table 3. Fault mechanism and hypocenter location (NCEDC, 2014)

Moment Magnitude (**M**)	6.02
Fault strike (deg)	155
Fault dip (deg)	82
Fault rake (deg)	172
Hypocenter Latitude (deg)	38.20837
Hypocenter Longitude (deg)	-122.29894
Hypocenter Depth (km)	10.117

Table 4. Rectangular Finite fault models used in this study (Boatwright 2014)

Corner	Latitude (deg)	Longitude (deg)	Depth (km)
1	38.2200	-122.3130	0.0000
2	38.3100	-122.3331	0.0000
3	38.3100	-122.3330	11.0000
4	38.2200	-122.3131	11.0000

For site conditions, the site database developed by PEER during NGA-West2 study was used (Seyhan et al. 2014). From the NGA-West2 site database, site parameters such as V_{s30}, $Z_{1.0}$ and $Z_{2.5}$ were obtained for 98 stations out of the 214. For 116 stations, for which we did not have V_{s30} values, the estimated values were computed (Gutierrez 2014, personal communication) according to the methodology described by Seyhan et al. (2014). V_{s30} for the selected stations were also estimated from Geomatrix 3rd letter and by the method by Wald and Allen (2007). $Z_{1.0}$ and $Z_{2.5}$ are estimated from V_{s30} as described in Chiou and Young (2014) and Campbell and Bozorgnia (2014), respectively. Based on this approach, these site condition metadata were estimated for all 214 stations. As a result, the number of stations belonging to site class A, B, C, D, and E (ASCE 2010) are 0, 8, 126, 75, and 5, respectively. The median V_{s30} of all sites is 490 m/s, which will be used in the following section as reference V_{s30} to compare the recorded PSA to GMPE predictions.

1.4.2 Comparison of Pseudo-Spectral Acceleration (PSA) to Ground-Motion Prediction Equations (GMPEs)

The 5%-damped PSA for the motions recorded at the stations listed in Table 1 were compared to the 2014 NGA-West2 GMPEs (Abrahamson et al. 2014 [ASK14], Boore et al. 2014 [BSSA14], Campbell and Bozorgnia 2014 [CB14], and Chiou and Youngs 2014 [CY14]) by using the appropriate distance metrics and site conditions described in the previous sections. Figure 7 shows the horizontal PSA based on RotD50 compared with the weighted geometric mean of the GMPEs (ASK14, BSSA14, CB14, and CY14 with equal weight). The results show that the PGA predicted by the GMPEs match well with the recorded values except Carquinez Bridge Geotechechnical Array #1 and #2 shown in Figure 7(c) and (d). This observation indicates that the amplification of high frequency content described in the previous section is larger than the site effects expected from GMPEs by V_{s30}. It is also observed that the GMPEs tend to underestimate the PSA at periods greater than 0.5 s at Lovall Valley Loop Rd and Napa Fire Station No. 3 in Figure 7(e) and (f). These stations are located at northern edge of the fault model as shown in Figure 3. It is also observed that GMPEs do not capture the pulse observed at a period of 1.5 seconds for the Napa College records in Figure 7(a).

Figure 8 shows the vertical PSA compared with the GMPE by Bozorgnia and Campbell (, 2014**)**. The comparisons show a general satisfactory agreement between recorded and estimated values, especially at the short vertical periods that are important for the vertical component, with the following exceptions. Figure 8 shows that PGA are underestimated for Carquinez Br Geotech Array #1 and #2 in Figure 8(c) and (d). Similarly, PSA greater than 1 s are underestimated at Lovall Valley Loop Rd and Napa Fire Station No. 3 in Figure 8(e) and (f). These trends observed in vertical PSA are similar to those observed in horizontal PSA.

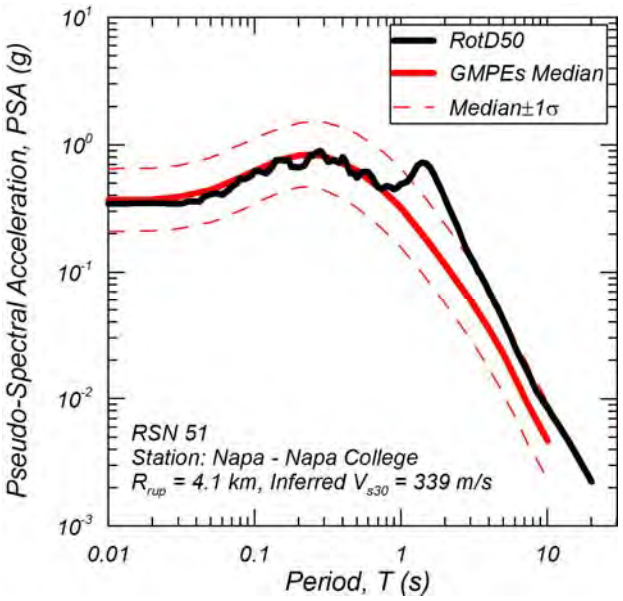

(a) Napa College

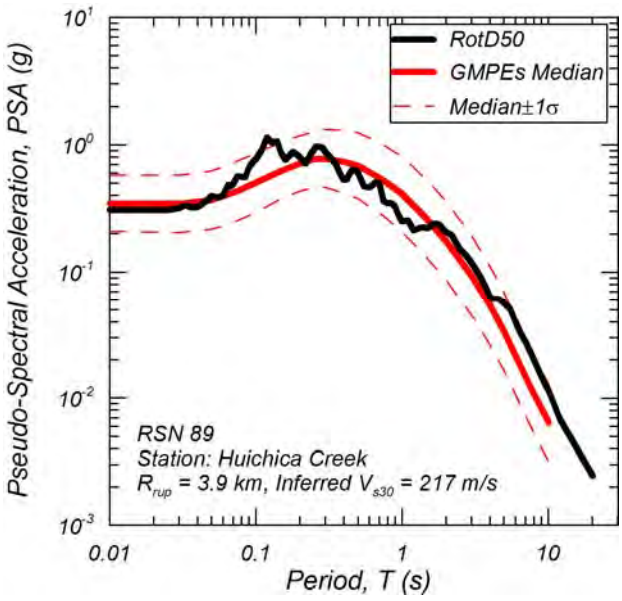

(b) Huichica Creek

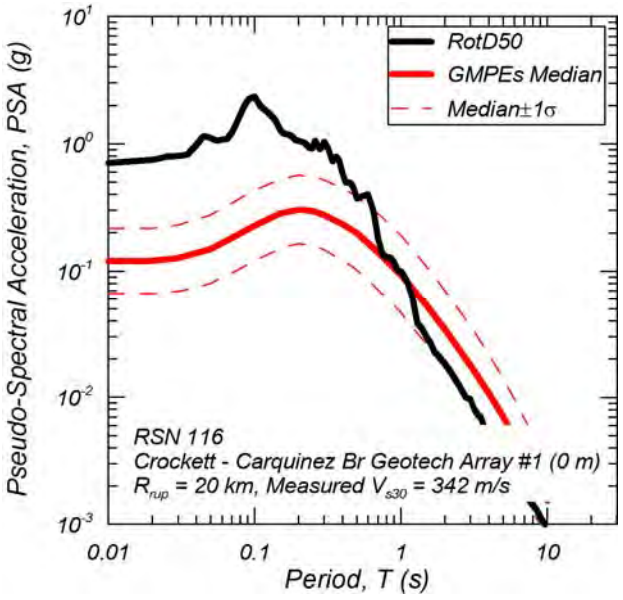

(c) Carquinez Br Geotech Array #1

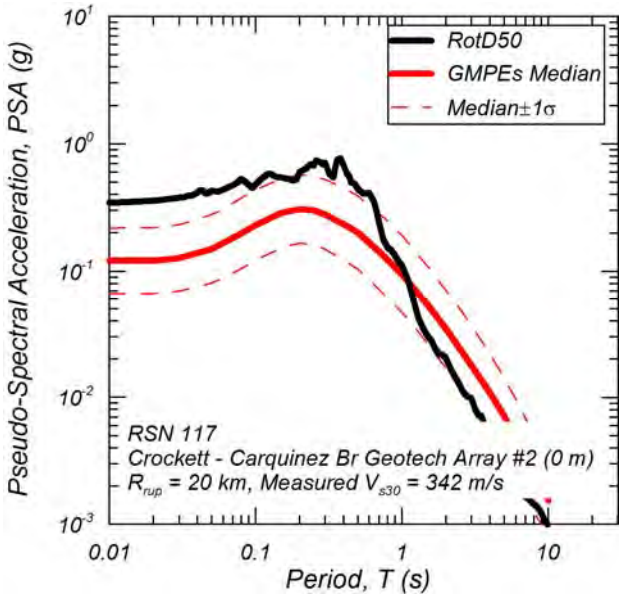

(d) Carquinez Br Geotech Array #2

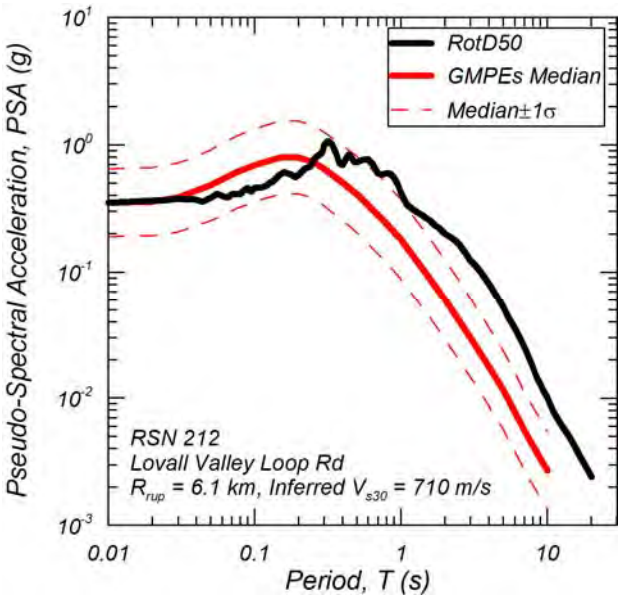

(e) Lovall Valley Loop Rd

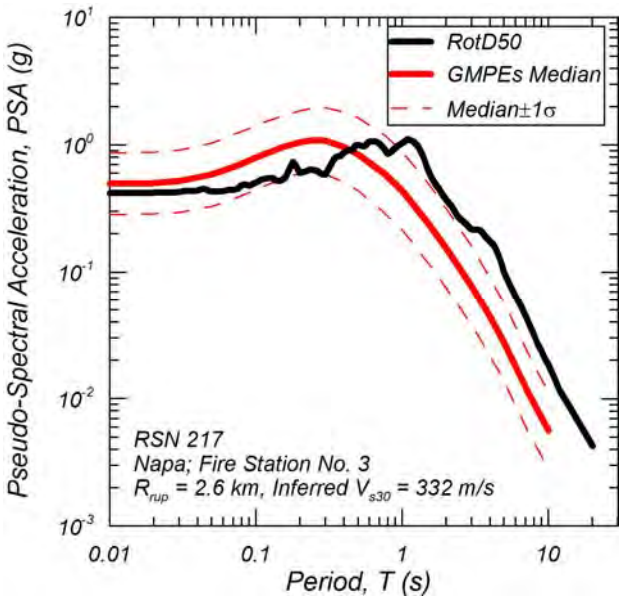

(f) Napa Fire Station No. 3

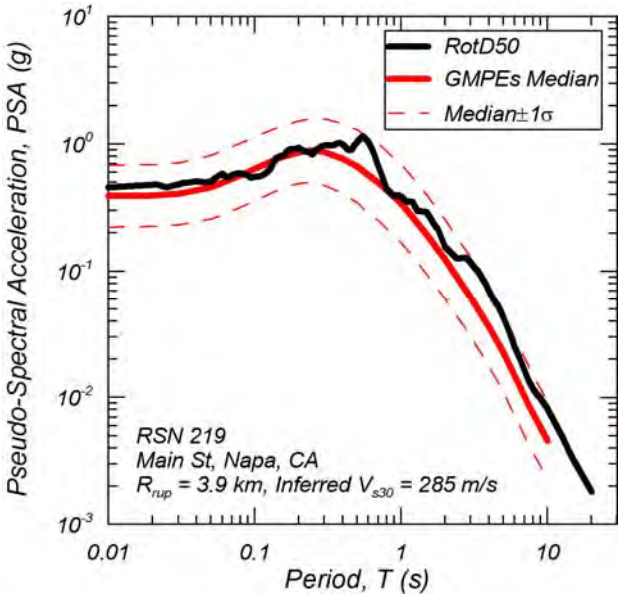

(g) Main St. Napa

Figure 7 Horizontal PSA (RotD50) compared to mean NGA-West2 GMPEs (2014)

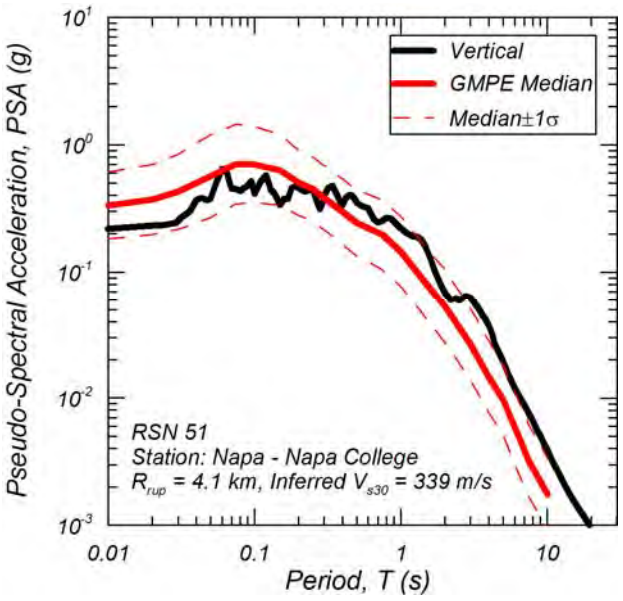

(a) Napa College

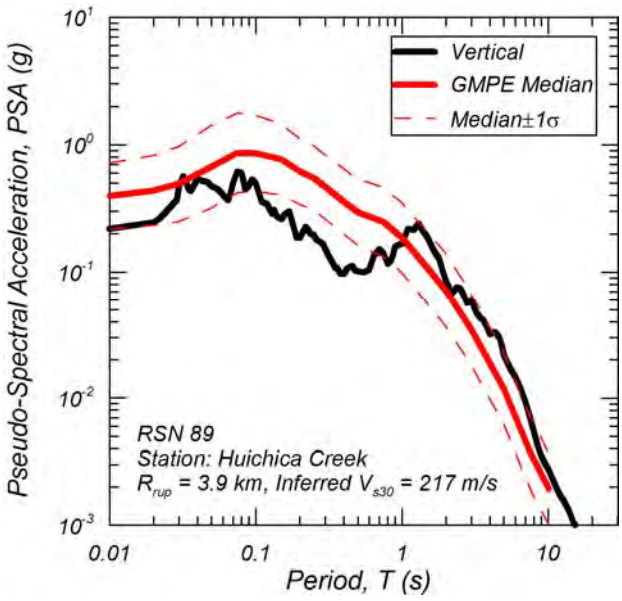

(b) Huichica Creek

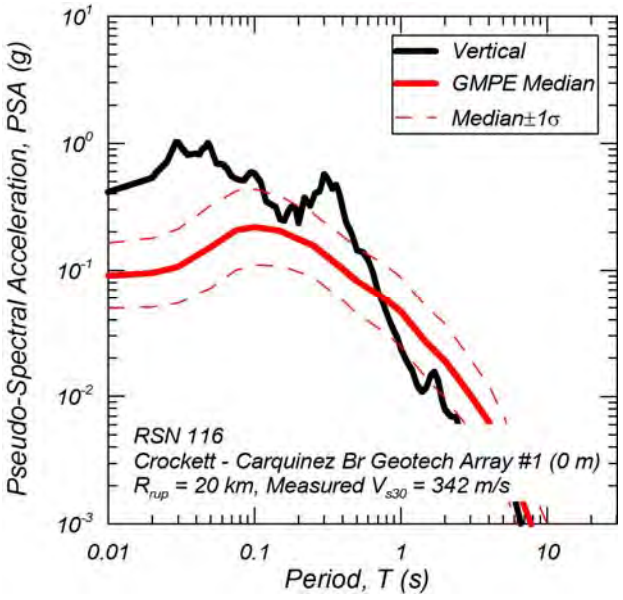

(c) Carquinez Bridge Geotechnical Array #1

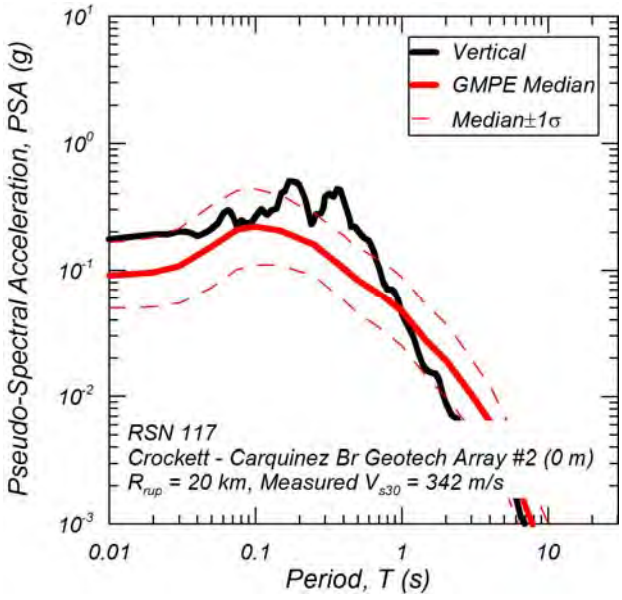

(d) Carquinez Bridge Geotechnical Array #2

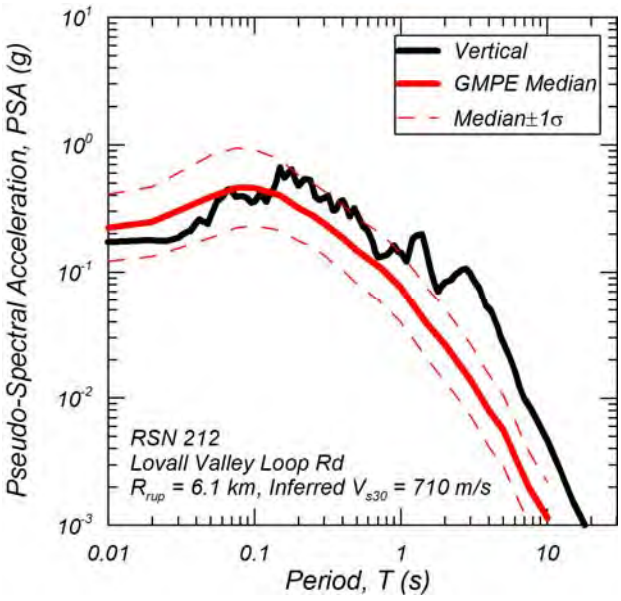

(e) Lovall Valley Loop Rd

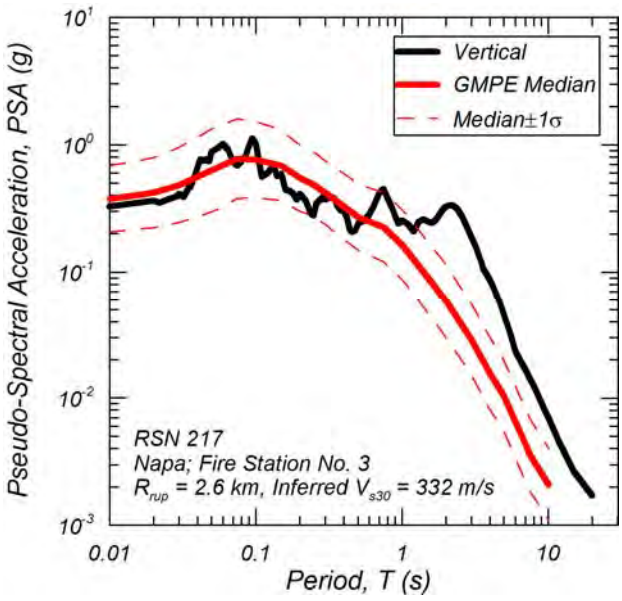

(f) Napa Fire Station No. 3

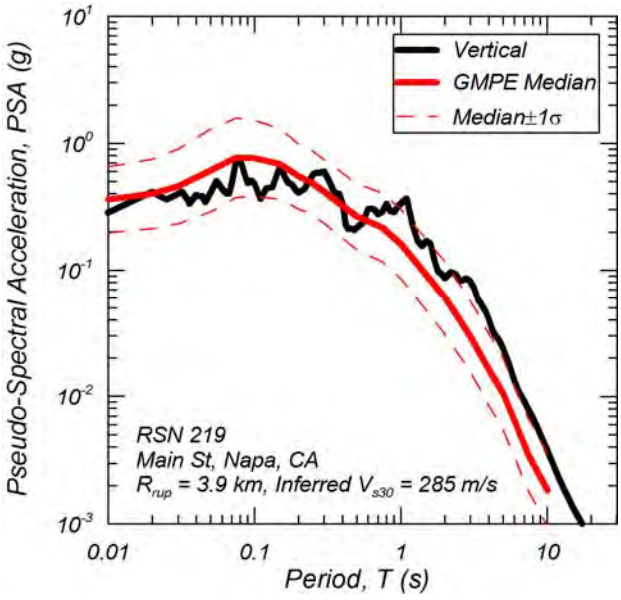

(g) Main St. Napa

Figure 8 Vertical Acceleration Resposne Spectra compared to Bozorgnia and Campbell (2014)

Horizontal PSA for all the stations were compared to the predicted median values obtained by taking the geometric mean of ASK14, BSSA14, CB14, and CY14. Figure 9 shows the comparison of PGA, PSA at T=0.2 s (PSA(0.2)), PSA at T=1.0 s (PSA(1.0)), and PSA at T=3.0 s (PSA(3.0)) against R_{rup} where the V_{s30} of 490 m/s is used in the GMPEs. The PSA of the records were adjusted to a reference V_{s30} of 490 m/s by V_{s30} scaling to these records. The figures show that PGA and PSA(0.2) are reasonably predicted within R_{rup} of 10 km whereas PSA(1.0) is underpredicted for this range. At distances greater than about 10 km the median GMPE tends to overpredict PGA and spectral values at 0.2 and 1.0 sec.

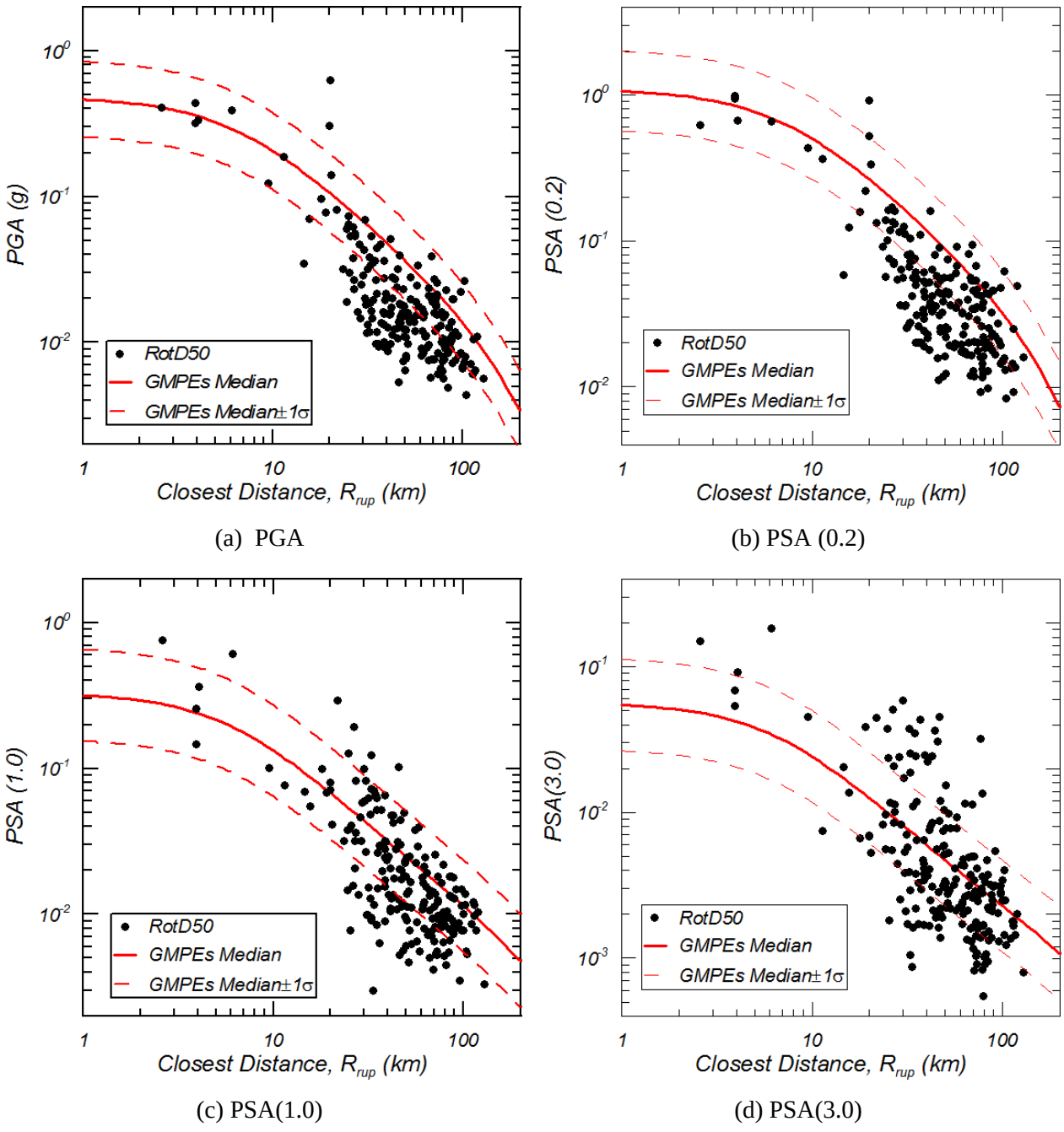

(a) PGA

(b) PSA (0.2)

(c) PSA(1.0)

(d) PSA(3.0)

Figure 9 Comparison of horizontal PSA (RotD50) with GMPEs against R_{rup}

Figure 10 shows the within-event residuals of PGA, PSA(0.2), PSA(1.0) and PSA(3.0) against R_{rup} after subtracting the event terms from the residuals. Event terms were computed for R_{rup} less than 50 km. The figures show that the event terms are negative for all parameters indicating that the ground shaking was lower than the median predicted by the GMPEs.

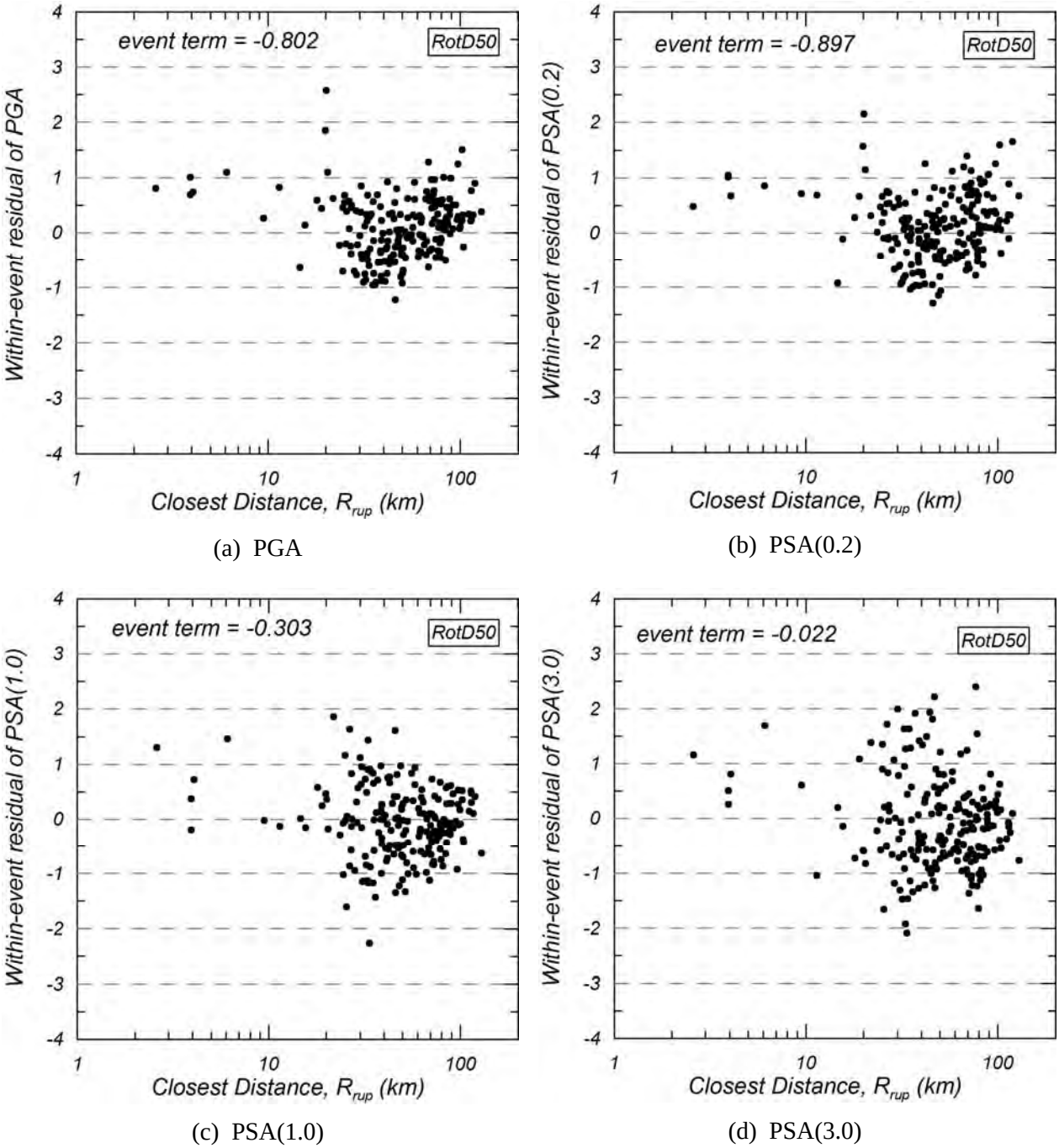

(a) PGA (b) PSA(0.2)

(c) PSA(1.0) (d) PSA(3.0)

Figure 10 Within-event residuals of horizontal PSA (RotD50) with GMPEs against R_{rup} (event term was computed within R_{rup} of 50 km.)

Vertical PSA were compared to the predicted values obtained by Bozorgnia and Campbell (2014). Figure 11 shows the comparison of PGA, PSA(0.2), PSA(1.0) and PSA(3.0) against R_{rup} where V_{s30} of 490 m/s is used in the GMPE. The PSA of the records were also adjusted to a V_{s30} of 490 m/s, as was done for the horizontal records. The comparison shows that PSA are reasonably estimated within R_{rup} of 10 km, although it shows an underestimation for PSA(1.0) and PSA(3.0).

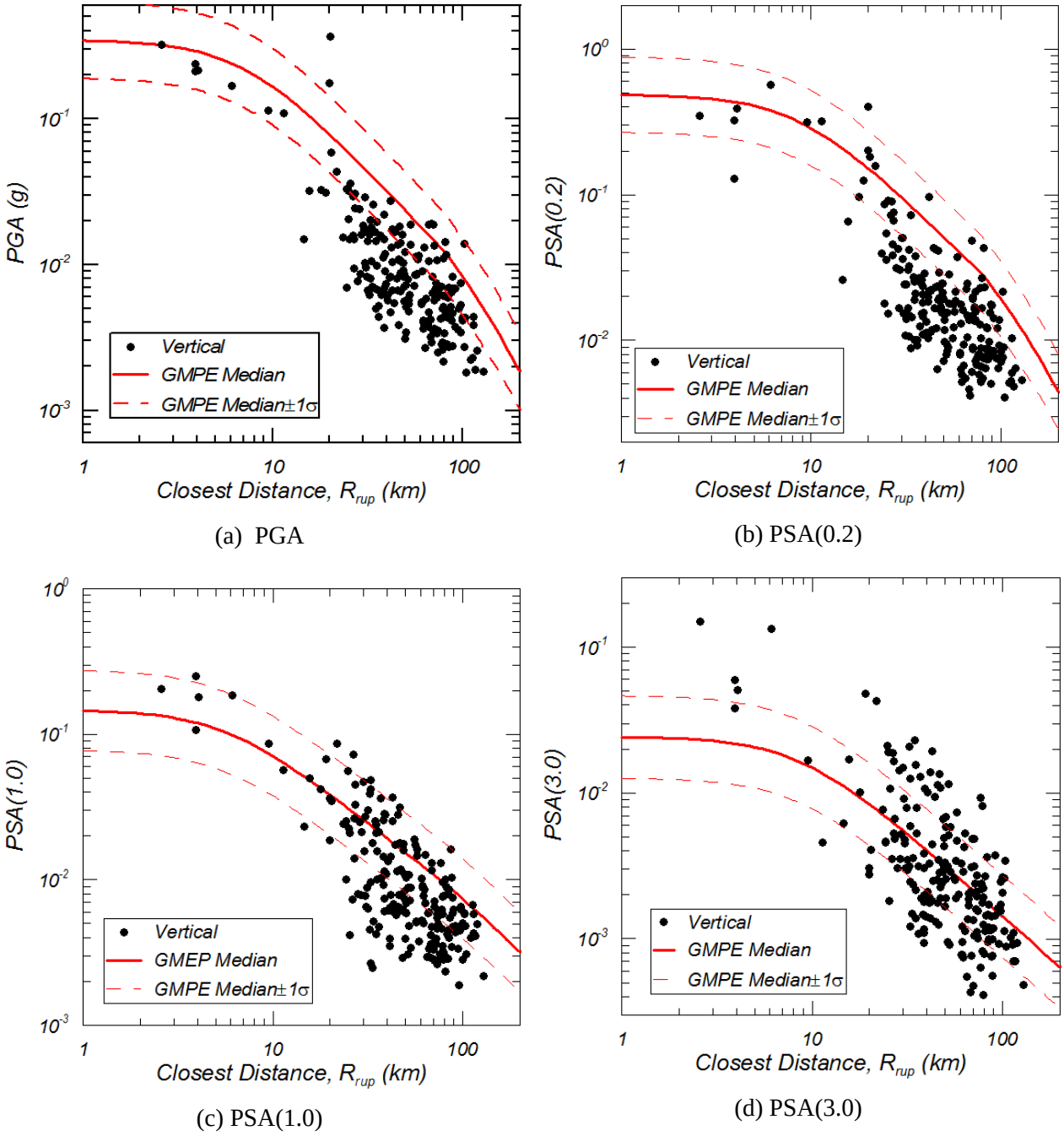

(a) PGA

(b) PSA(0.2)

(c) PSA(1.0)

(d) PSA(3.0)

Figure 11 Comparison of vertical PSA with GMPE against R_{rup}

Figure 12 shows the within-event residuals of PGA, PSA(0.2), PSA(1.0), and PSA(3.0) against R_{rup} after subtracting the event term from the residuals. Event terms were computed for R_{rup} less than 50 km. The figures show that the event terms are negative for all PSA indicating that the ground shaking was lower than the median values predicted by the GMPE.

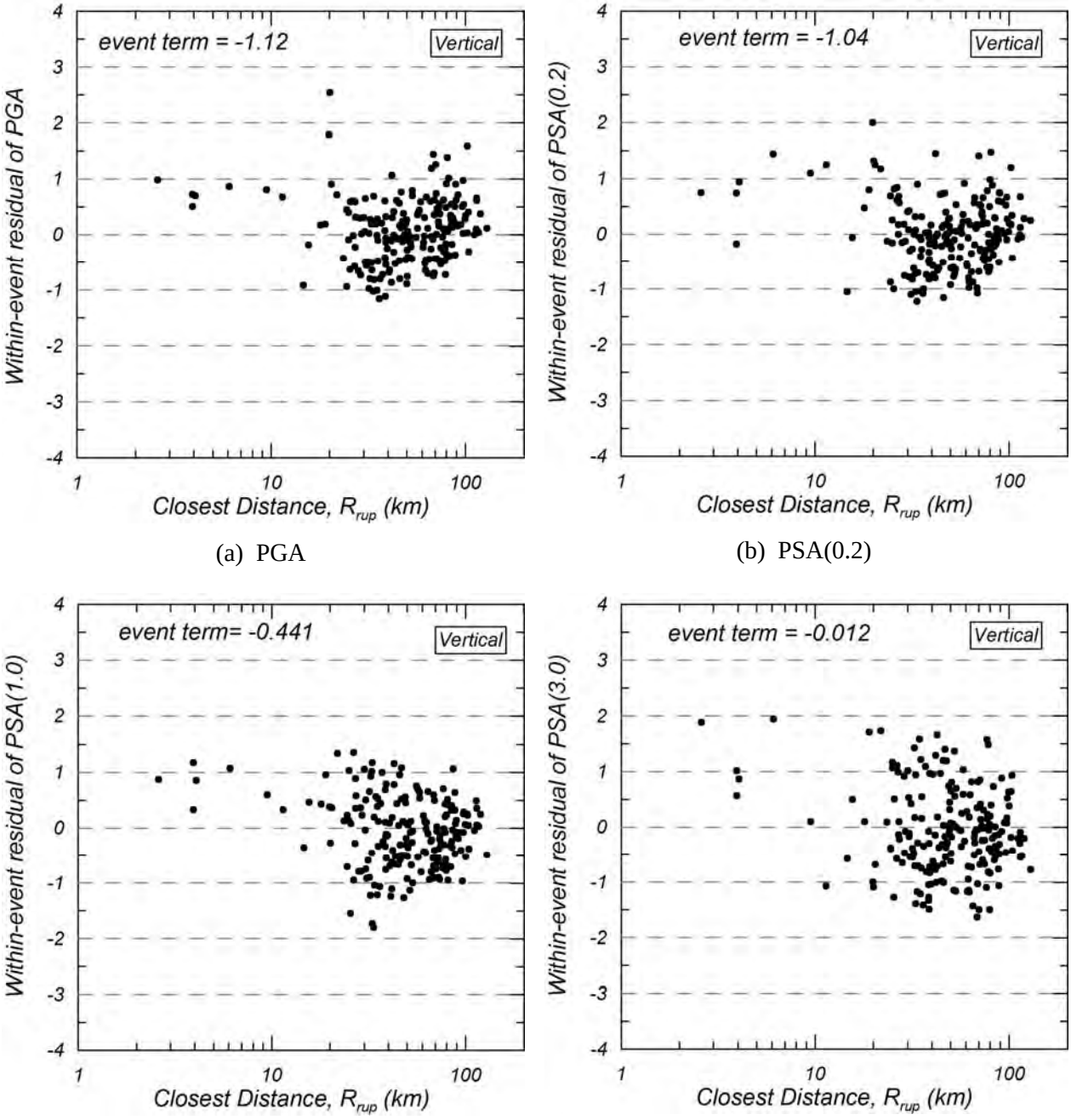

(a) PGA (b) PSA(0.2)

(c) PSA(1.0) (d) PSA(3.0)

Figure 12 Within-event residuals of vertical PSA with GMPE against R_{rup} (event term was computed within R_{rup} of 50 km.)

1.5 COMPARISON OF RECORD RESPONSE SPECTRA TO CODE-BASED DESIGN SPECTRA

In this section, the 5% damped acceleration response spectra of the recorded ground motions are compared to the various code-based design spectra. Two sets of plots are presented. The first set directly compares the three recorded components with the code spectra. The second set compares the processed spectra with the code-based spectra; this comparison is for design purposes with respect to certain ground motion selection requirements documented in ASCE 7-10. In addition, the pseudo-spectral acceleration, Uniform Hazard Response Spectra (UHRS), and displacement spectra for different return periods are presented for Napa College, Napa Main Street, Napa Fire Station No. 3, and the surface recording from the Vallejo-Hwy 37 Geotechnical Array. Similar plots for the other stations listed in Table 1 are presented in Appendix C. All the spectra presented in this section correspond to a 5% damping ratio.

1.5.1 Design Spectra

The design spectra for buildings were constructed based on ASCE 7-10, Chapter 11, while the Caltrans Seismic Design Criteria, Appendix B (version 1.7, 2013), was used to construct the design spectra for bridges, such as Highway 37/Napa Valley Bridge.

1.5.1.1 ASCE 7-10 Design Spectra for Buildings

The site class for each station is determined based on the site's estimated V_{s30} value, as discussed in section 1.4.1. The risk-targeted mapped acceleration parameters such as S_{d1}, S_{ds}, S_{m1}, S_{ms} were obtained using the USGS Seismic Design Maps online tool: http://earthquake.usgs.gov/designmaps/us/application.php. With those values, the design spectra for Design Based Earthquake (DBE) and Maximum Considered Earthquake (MCE) were constructed for different period ranges. The period range is 0 to 3.0 second for all spectra plotted in this chapter, because this range covers nearly all of the fundamental periods for structures in built-up areas in Napa.

1.5.1.2 Caltrans Design Spectra for Bridges

The Caltrans design spectrum was based on the envelope of a deterministic and probabilistic spectrum for each location. The deterministic spectrum was calculated as the arithmetic average of the median response spectra calculated using CB08, CY08, and the probabilistic spectrum was obtained from the USGS Seismic Hazard Map (Petersen et al, 2008) for the 5% in 50 year probability of exceedance (975 year return period) taking into account of the spectrum adjustment factors due to near-fault effects, basin effects, etc. Site specific analyses are also required if the soil profile includes soft clay deposits.

1.5.2 Resultant Spectra

The Square Root Sum of Squares (SRSS) of the two horizontal components was calculated for each recording station. Additional resultants, such as the RotD50 (median rotated component) and RotD100 (maximum rotated direction component), were also calculated (Boore et al. 2010).

1.5.3 UHRS

Another set of plots comparing the median-rotated component and UHRS for different hazard levels are also included. The UHRS for selected station were calculated using the USGS online tool: http://geohazards.usgs.gov/hazardtool/application.php.

Station Name: Napa College

V_{s30}(m/sec): 339

Soil Type: D

PGA: 0.344 g

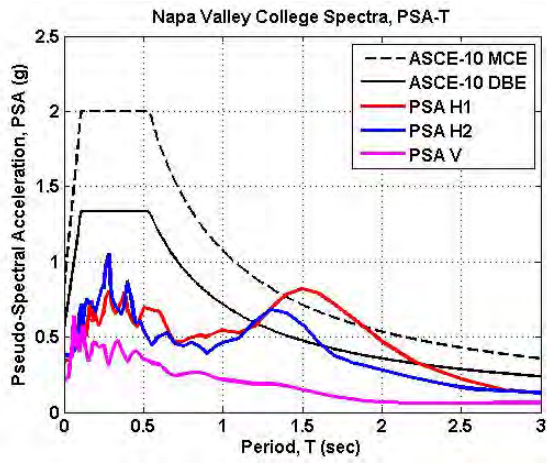

(a). Code-based vs. as-recorded PSA

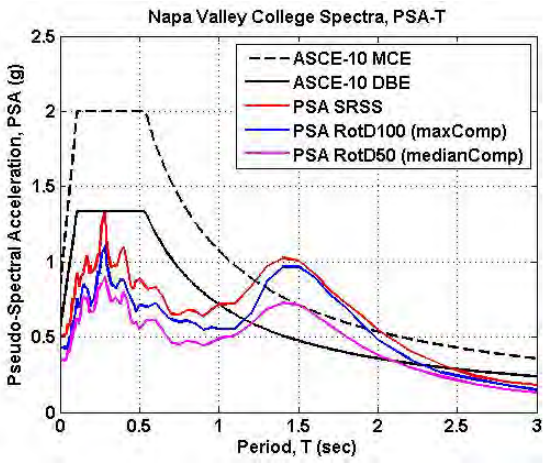

(b). Code-based vs. resultant PSA

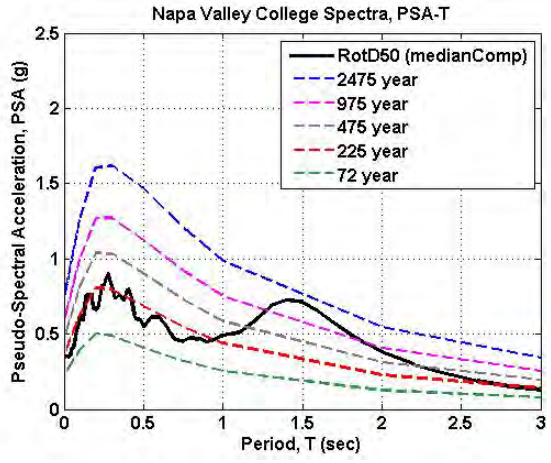

(c). UHRS vs. median component PSA

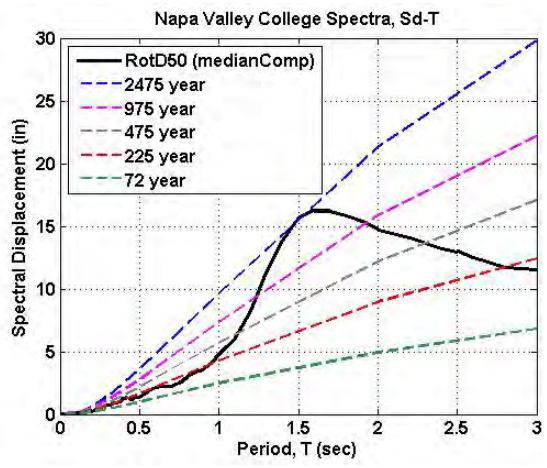

(d). UHRS vs. median component Sd

Figure 13 Spectra comparison for Napa Valley College

Station Name: Napa Main Street

V_{s30} (m/sec): 285

Soil Type: D

PGA: 0.445 g

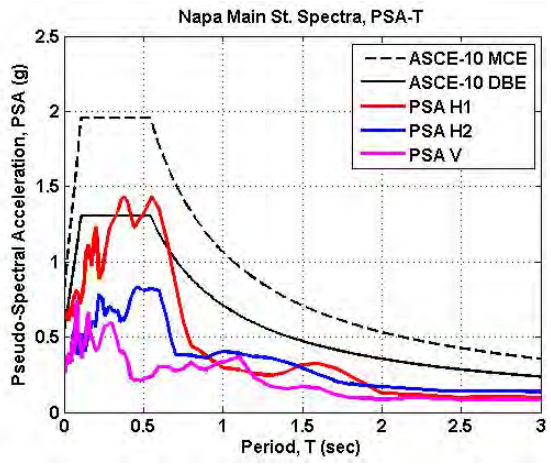

(a). Code-based vs. as-recorded PSA

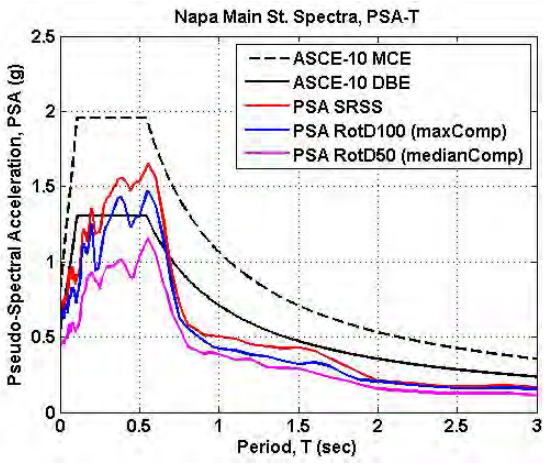

(b). Code-based vs. resultant PSA

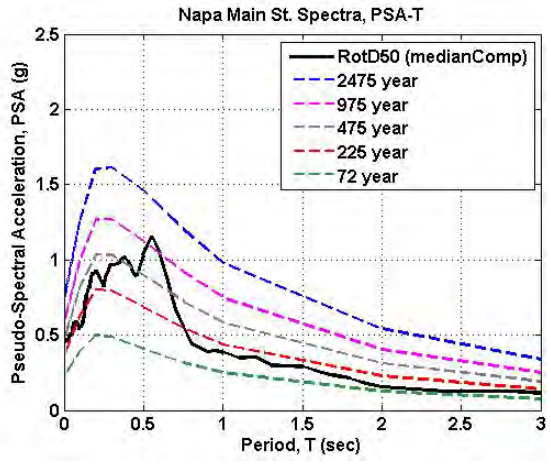

(c). UHRS vs. median component PSA

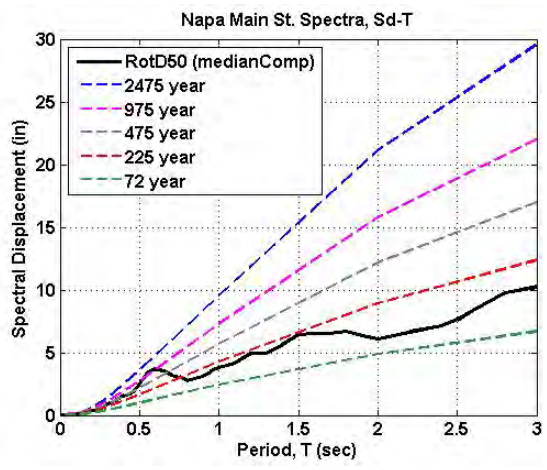

(d). UHRS vs. median component Sd

Figure 14 Spectra comparison for Napa Main Street

Station Name: Napa; Fire Station No. 3

V_{s30} (m/sec): 332

Soil Type: D

PGA: 0.346 g

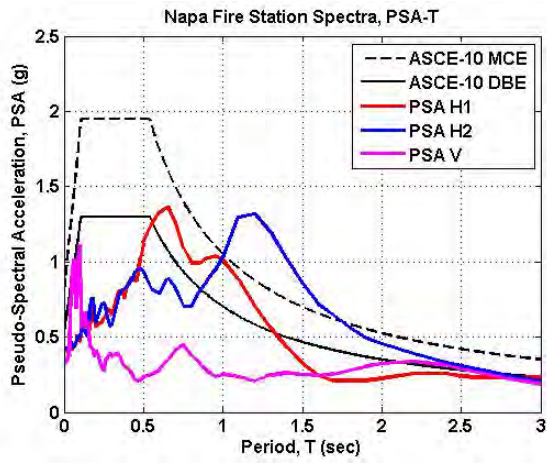

(a). Code-based vs. as-recorded PSA

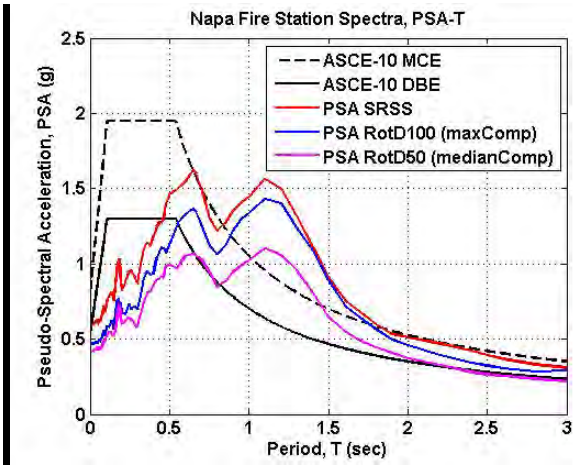

(b). Code-based vs. resultant PSA

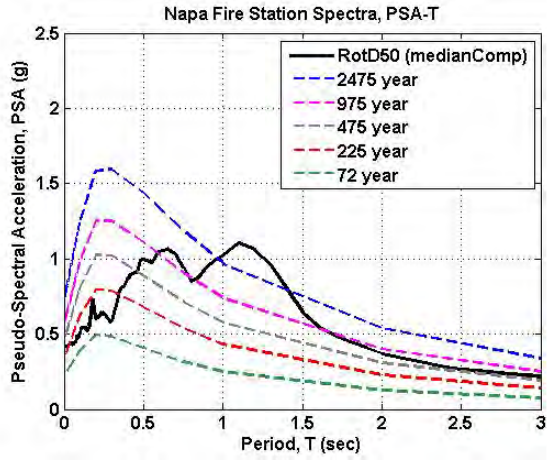

(c). UHRS vs. median component PSA

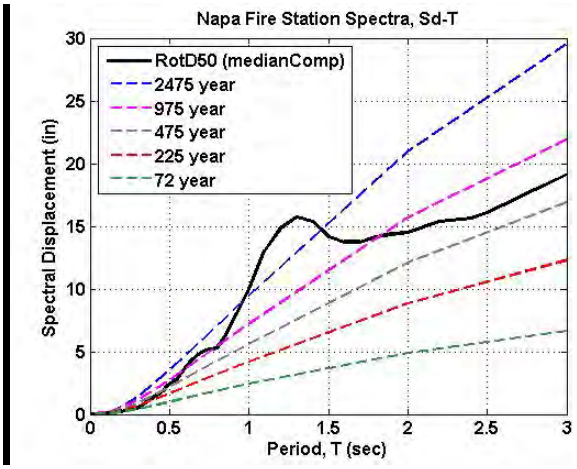

(d). UHRS vs. median component Sd

Figure 15 Spectra comparison for Napa; Fire Station No. 3

Station Name: Vallejo - Hwy 37/Napa River E Geotech Array (0m)

V_{s30} (m/sec): 509

Soil Type: C

PGA: 0.198 g

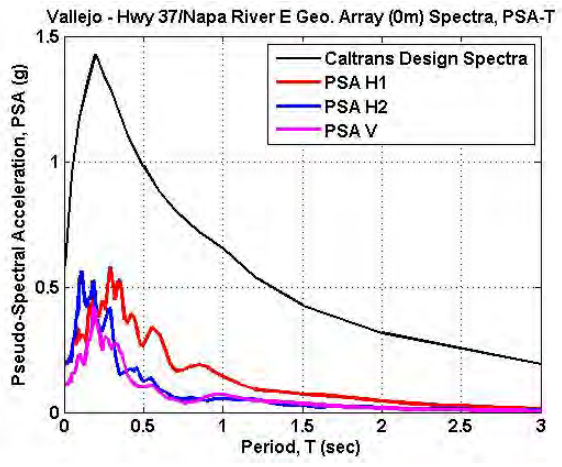

(a). Code-based vs. as-recorded PSA spectra

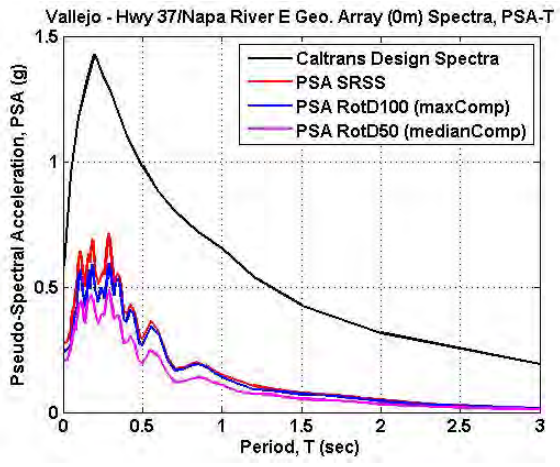

(b). Code-based vs. resultant PSA spectra

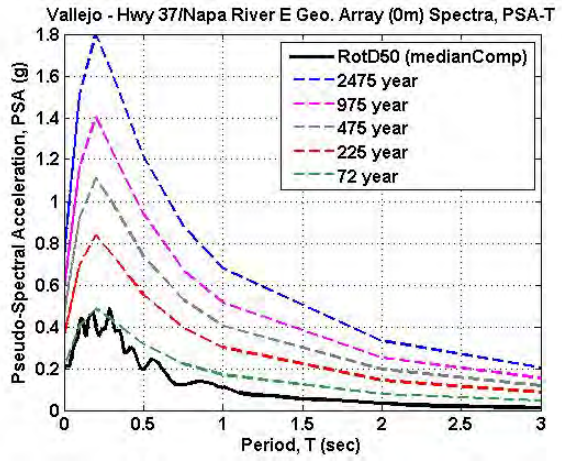

(c). UHRS vs. median component PSA

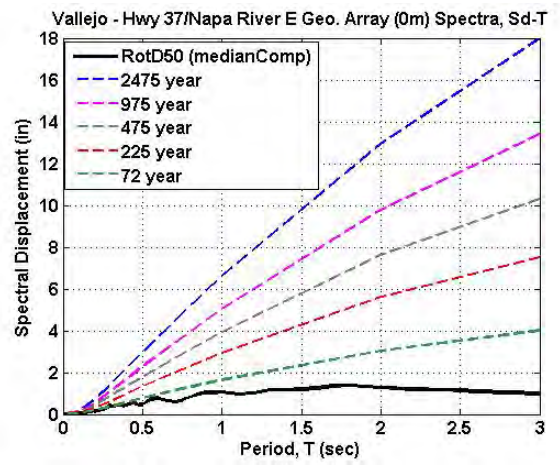

(d). UHRS vs. median component Sd

Figure 16 Spectra comparison for Vallejo - Hwy 37/Napa River E Geotech Array (0m)

1.6 SUMMARY OF GROUND MOTION OBSERVATIONS

This report summarizes a preliminary study on the characteristics of the strong-motion recordings from the South Napa Earthquake of August 24th, 2014. The strong-motion data were downloaded from CESMD website and processed following the PEER standard data processing methodology. Associated metadata such as source-to-site distances and estimated site parameters such as V_{s30} were estimated following the approached developed in the PEER NGA-West2 study. Strong ground motions were observed within Napa Valley where PGA values greater than 0.3 g were recorded.

Velocity pulses were observed near the fault for which five time series were examined by using the approaches by Hayden et al. (2014) and Shahi (2013). The results show that these records were classified as pulse-type motions in the near-fault region even though a discrepancy between these approaches exists for the Main St. Napa and Napa College stations.

Four near fault ground motions were similarly characterized using the proposed method by Lu and Panagiotou (2014) (Napa Fire Station No. 3, Napa Main St., Fault Normal and Fault Parallel directions). Analyses showed that each of the records includes more than one strong long-period pulse with the predominant period (T_P) of the multiple pulses to differ significantly. The T_P of the long-period pulses ranged between 0.8 and 3.9 s. All four ground motions, included two strong long-period pulses of significantly different T_P that were well correlated in the time domain. All motions also included strong short-period pulses ($T_P < 0.6$ s).

High-frequency spikes were observed in the records at Carquinez Bridge Geotechnical Array #1 which reached approximately 1.0 g for the NS component. These spikes were investigated by comparing the acceleration time series at several stations along the path from the epicntert to the sites and the downhole array records. These spikes were observed in the S-wave portion of the records based on visual inspection. Acceleration time series along the source to site travel path shows the similar spikes at the recordings at Napa College, Vallejo – Hwy 37/Napa River East Geotechnical Array, and Carquinez Bridge Geotechnical Arrays #1 and #2. This suggests that the spikes could be a result of path effects. The spikes increase in amplitude from Vallejo – Hwy 37/Napa River East Geotechnical Array to Carquinez Bridge Geotechnical Array #1. Downhole records show that two high frequency spikes are observed in the S-wave portion of the waveform from a depth below 100 m to the surface. This observation may indicate that the large PGA observed at Carquinez Bridge Geotechnical Array #1 could also be the result of site amplification through the soft soil deposits. However, these observations do not exclude the possibility of soil-structure interaction effects on the measured recordings. Further investigation is recommended to study the observed high-frequency content near the Carquinez Bridge.

The pseudo-spectral accelerations (5% damped) from the recorded ground motions were compared to the recent NGA-West2 GMPEs for PGA, 0.2, 1.0 and 3.0 seconds. The comparison shows generally a good agreement for both of horizontal and vertical components near the fault with the exception of the large high frequency motions observed near the Carquinez Bridge.

Recorded ground motions were also compared to the code-based design spectra. The comparison shows that the pseudo-spectral accelerations recorded at Napa College and Napa Fire Station No. 3 exceeded the MCE design spectra at a period around 1.5 s near the fault. This observation is related to the near-fault velocity pulses discussed in the report. The comparison also shows that the pseudo-spectral acceleration recorded at Carquinez Bridge exceeded the Caltrans design spectra for short periods. This observation is related to the amplification of high frequency spikes discussed in the report. Further investigation is recommended to study the damage observations related to the recorded ground motions and design spectra. There needs to be more researchinto which pulse featuresmay have damaging effects on elastic and inelastic systems.

1.7 REFERENCES

Abrahamson, N. A., Silva W. J., and Kamai, R., 2014. Summary of the Abrahamson, Silva, and Kamai NGA-West2 ground-motion relations for active crustal regions, Earthquake Spectra, EERI, Pre-Print.

Abrahamson, N., Atkinson, G., Boore, D., Bozorgnia, Y., Campbell, K., Chiou, B, Idriss, I.M., Silva, W. and Youngs, R., 2008. Comparisons of NGA Ground-Motion Relations, Earthquake Spectra, EERI, Vol. 24, No. 1, Feb., pp. 45-66.

Ancheta, T. D., Darragh, R. B., Stewart, J. P., Seyhan, E., Silva, W. J., Chiou, B. S. J., Wooddell, K. E., Graves, R. W., Kottke, A. R., Boore, D. M., Kishida, T., Donohue, J. L., 2014, PEER NGA-West2 Database. Earthquake Spectra, EERI, Pre-Print.

Boore, D. M, 2010. Orientation-independent, nongeometric-mean measures of seismic intensity from two horizontal components of motion, Bull. Seismol. Soc. Am., 100, 1830 – 1835.

Boore, D. M., Stewart, J. P., Seyhan, E., and Atkinson, G. A., 2014. NGA-West2 equations for predicting response spectral accelerations for shallow crustal earthquakes, Earthquake Spectra, EERI, Pre-Print.

Bozorgnia, Y., and Campbell, K.W., 2014. Vertical ground motion model using NGA-West2 database, Earthquake Spectra, EERI, submitted.

Bray, J.D., Rodriguez-Marek, A., and Gillie, J. L., "Design Ground Motions Near Active Faults," Bulletin of the New Zealand Society for Earthquake Engineering, 42 (1), March, 2009, 8 pp.

Campbell, K. W. and Y. Bozorgnia (2008), "NGA ground motion model for the geometric mean horizontal component of PGA, PGV, PGD and 5% damped linear elastic response spectra for periods ranging from 0.01 to 10s", Earthquake Spectra, 24(1), 139-171.

Campbell, K. W., and Bozorgnia, Y., 2014. Campbell-Bozorgnia NGA-West2 ground motion model for the average horizontal components of PGA, PGV, and 5%-damped linear Response Spectra, Earthquake Spectra, EERI, Pre-Print.

Chiou, B. S. J., and Youngs, R. R., 2014. Update of the Chiou and Youngs NGA ground motion model for average horizontal component of peak ground motion and response spectra, Earthquake Spectra, EERI, Pre-Print.

Chiou, B. S.-J. and Youngs R. R. (2008), An NGA model for the average horizontal component of peak ground motion and response spectra, Earthquake Spectra, 24(1), 173-215.

Hayden, C.P., Bray, J.D., and Abrahamson, N.A. (2014). "Selection of Near-Fault Pulse Motions." J. Geotech. Geoenviron. Eng., 140(7), 04014030.

Lu, Y., and Panagiotou, M. (2014). "Characterization and Representation of Near-fault Ground Motions Using Cumulative Pulse Extraction with Wavelet Analysis," *Bulletin of the Seismological Society of America*, 104:410-426.

Petersen, M.D., Frankel, A. D., Harmsen, S. C., Mueller, C. S., Haller, K. M., Wheeler, R. L., R. L. Wesson, Zeng, Y., Boyd, O. S., Perkins, D. M., Luco, N., Field, E. H., Wills, C. J. and Rukstales, K. S. "Documentation for the 2008 Update of the United States National Seismic Hazard Maps", USGS, Open-File Report 2008–1128.

Shahi, S. (2013). “A probabilistic framework to include the effects of near-fault directivity in seismic hazard assessment.” Ph.D. Thesis, Stanford University, Stanford, CA.